Experiments on Vibrated Granular Materials: Waves, Convection and Segregation

A Thesis

Submitted for the Degree of

Master of Science (Engineering)

by

Mohammed Istafaul Haque Ansari

Engineering Mechanics Unit
Jawaharlal Nehru Centre for Advanced Scientific Research
(A Deemed University)
Bangalore – 560 064

AUGUST 2012

To my family

DECLARATION

I hereby declare that the matter embodied in the thesis entitled "**Experiments on Granular Fluid and Convection**" is the result of investigations carried out by me at the Engineering Mechanics Unit, Jawaharlal Nehru Centre for Advanced Scientific Research, Bangalore, India under the supervision of Prof. Meheboob Alam and that it has not been submitted elsewhere for the award of any degree or diploma.

In keeping with the general practice in reporting scientific observations, due acknowledgment has been made whenever the work described is based on the findings of other investigators.

Mohammed Istafaul Haque Ansari

CERTIFICATE

I hereby certify that the matter embodied in this thesis entitled "**Experiments on Granular Fluid and Convection**" has been carried out by Mr. Mohammed Istafaul Haque Ansari at the Engineering Mechanics Unit, Jawaharlal Nehru Centre for Advanced Scientific Research, Bangalore, India under my supervision and that it has not been submitted elsewhere for the award of any degree or diploma.

Prof. Meheboob Alam
(Research Supervisor)

Acknowledgements

First and foremost I would like to thank and express my sincere gratitude to my research advisor *Prof. Meheboob Alam*. He showed me, with an always encouraging, inspiring and supporting guidance, through the fascinating new world of granular flow. His deep knowledge of granular flow and fluid mechanics helped me a lot during my research work. I am really indebted and fortunate to have him as my research advisor.

I would like to thank all the professors whose courses I have attended, Prof. Meheboob Alam, Prof. K.R. Sreenivas, Prof. Rama Govindarajan, Dr. Santosh Ansumali, and Prof. S.M. Deshpande. I thank Dr. Ganesh Subramanian for allowing me to attend his Microhydrodynamics class (although I was not able to attend all the classes).

I am thankful to *Prof. A.K. Srivastava* (my engineering college HOD), for motivating me towards research that helped me to find my way to JNCASR.

I am grateful to JNCASR for providing financial support, very good infrastructural facilities and a wealthy library. I would like to thank the administrative, technical and Complab staff, whose job keeps our daily life moving smoothly in JNC.

I thank my lab alumni Priyanka, Vinay and lab mates Sunil, Rohan, Ujjayan, Ramkrishna, Reddy, Deepthi, Saikat, Arijeet and other friends in EMU for their help during my stay in JNC. I thanks Ershad and Rukhsan (TSU) for their support and help.

I would like to thank my parents, sister, brothers and brother-in-law, with whom I share all my joys, whose love saw me through testing times, and who have stood by me no matter what.

Abstract

Granular materials under vertical shaking exhibit a variety of interesting phenomena: undulations, surface instabilities, oscillons, ripples, granular Leidenfrost state and convection. In this thesis we have investigated these phenomena by conducting experiments on both monodisperse system (glass balls of diameter 1.0 mm) and two bidisperse mixtures: (a) the glass and steel balls both having diameters of 1.0 mm and a density ratio of $\rho_s/\rho_g = 3.03$ and (b) the delrin and steel balls both having diameters of 1.0 mm and a density ratio of $\rho_s/\rho_d = 5.55$. The particles are held in a quasi-two-dimensional. Perspex® container which is vibrated harmonically using an electromagnetic shaker. The dimensionless control parameters involved in the experiments are: (i) the dimensionless shaking acceleration $\Gamma = A\omega^2/g$, where A is the shaking amplitude and $\omega = 2\pi f$ the angular frequency of shaking and d the diameter of balls, (ii) the number of particle layers at rest $F = h_0/d$ and (iii) the aspect ratio of the container L/h_0, where h_0 is the bed height at rest. The relevant control parameters have been identified for each observed phenomenon and the phase transitions between them. The experimental data have been assimilated to construct phase diagrams in the (Γ, F)-plane for different shaking amplitudes. The results on monodisperse system are compared and contrasted with previous experiments of Eshuis *et. al.* [7]. The results on binary mixtures are new and the influence of the density ratio of two types of particles on various patterns and segregation is discussed. For binary mixtures, we found many unhitherto reported novel patterns: (i) the Leidenfrost state coexisting with a granular gas, (ii) horizontal segregation within a Leidenfrost state, (iii) granular convection with a floating particle cloud, and (iv) both vertical and/or horizontal segregation with other patterned states. The phenomenon of "floating particle cloud" was found for the delrin and steel ball mixtures for a wide range of parameters beyond the bouncing bed regime.

List of Figures

Contents

CHAPTER 1

INTRODUCTION

1.1 Granular Matter

A *granular material* is a collection of solid particles or grains such that most of the particles are in contact with at least some of their neighboring particles. The terms granular materials, bulk solids, particulate solids and powders are used interchangeably in the literature. They occur in all shapes and sizes ranging from sand, gravel, food grains, seeds, sugar, coal, and cement to large planetry rings and asteroids. Granular materials are commonly encountered in nature as well as in various chemical processing industries. With reference to the chemical industry, Ennis *et. al.* note that about 40% of the value added is linked to particle technology [1]. Similarly, more than 50% of all products sold are either granular in form or involve granular materials in their production [2]. In spite of their importance, the mechanics of granular flow is not well understood at present. However, some progress has been made during the last few decades.

(a) Sand dunes

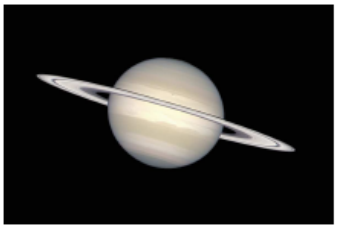

(b) Saturn ring

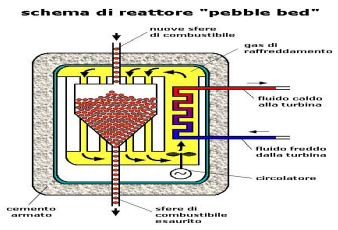

(c) Pebble bed nuclear reactor

(d) Coal

Figure 1.1: Examples of granular matter.

Granular matter can behave like all three states (gas, liquid and solid) of matter [3], [4] but they exhibit many features which cannot be anticipated on the basis of our experience with these states. They can sustain shear stresses at rest like solids as in the case of a sandpile. In a sandpile the inclination of the free surface of the heap to the horizontal is not arbitrary but decided by the *angle of repose*. They flow from vessels under the action of gravity like liquids, but the mass flow rate is approximately independent of the height of material above the discharge orifice; this feature accounts for the use of hourglasses containing sand as clocks a few centuries ago. They can behave like a gas as in the case of sand storm but unlike ordinary gases the collisions between particles of a granular gas are inelastic in nature. So, to sustain the gaseous state of granular matter energy must be continuously injected into te system as discussed in the experiments of this thesis. Overall, granular materials share some features of common fluids and solids but also differ from them in many ways. Various aspects of the behavior of granular materials have been discussed in review articles [5]- [4].

(a) (b) (c)

Figure 1.2: Behaviour of granular materials: (a) like a solid (sand castle), (b) like a liquid (flow of sand in an hour-glass), and (c) like a gas (sand storm).

A granular material is called a *dry* granular material if the fluids between the voids of the grains is a gas (air) whose density is much smaller than solid particles. If the voids are completely filled with a liquid such as water, the material is called a *saturated* granular material. If some of the voids are filled with air, and the rest are filled with a liquid, the material is said to be partially saturated. For example, the upper layer of soil in a natural environment is usually partially saturated, whereas the deeper layer is saturated.

1.2 Review on Patterns in Vibrated Granular Bed

Pattern formation on a vertically vibrated thin granular layer has been extensively studied experimentally [8]- [27]. We briefly review related literature in following subsections.

1.2.1 Various Surface Patterns in Vibrated Granular Material

Ripples and Undulatory Patterns: Ugawa *et. al.* [17] observed ripples and undulatory patterns on the surface of granular materials held in a rectangular cell of horizontal cross section $91 \times 8\ mm^2$ or $100 \times 2\ mm^2$. The container is vibrated sinusoidally

$$y = A\sin(2\pi ft), \tag{1.1}$$

where A is the amplitude of shaking and f is its frequency. The snapshots of spikes and undulation waves as reported by Ugawa *et. al.* [17] are shown in Fig. 1.3. These spikes are also called "f/4"-ripples since they repeat their maxima and minima positions in every four period of oscillation T, where T= $1/f$ is the period of oscillation.

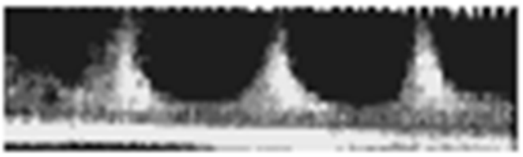

(a)

(b)

Figure 1.3: (a) Spikes ($f = 40Hz, A = 1.70\ mm, \Gamma = 11.0$), and (b) undulations ($f = 55Hz, A = 1.30\ mm, \Gamma = 15.8$) (taken from [17])

Clément *et. al.* [10] performed experiments with a bidimensional layer of aluminum beads of diameter 1.5 mm held in a two-dimensional (2D) container of widths

$L = 150\ mm$ and $300\ mm$. For large accelerations Γ, a surface instability shows up as an array of peaked structures separated by a wavelength λ (see Fig. 1.4). The characteristic of these surface instabilites are as follows: The characteristic of

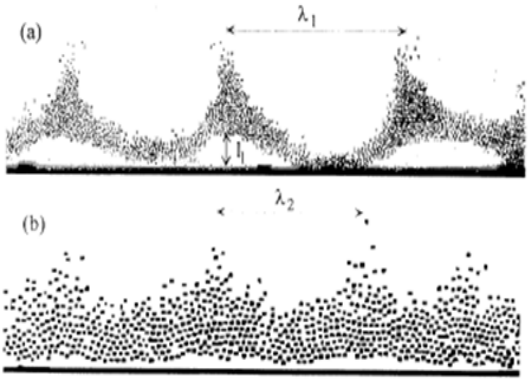

Figure 1.4: Snapshot of the surface instability for $N_h = 9$ layers of beads and dimensionless acceleration $\Gamma = 3.4$. The dots are the center of the beads.(a) $f = 7.8\ Hz$, (b) $f = 12\ Hz$. The pictures are not drawn at the same scale $\lambda_1 = 2\lambda_2$ (taken from [10]).

these surface instability are

- The arching height l between the bottom of the cell and the apex of the arch is indicated in the figure. In Fig. 1.4 (a), l_1 is of the order of several tens of bead sizes and in Fig. 1.4 (b) $l \simeq d$ i.e., the bead size.
- The maxima exhanges with minima in the next period, i.e. they are "f/2" waves.

Carrillo *et. al.* [19] numerically studied these subharmonic instabilities in a vertically vibrated granular layer and found that above a certain Γ, a periodic wave-like pattern appears with a frequency $f/2$. The snapshots of molecular dynamics (MD) simulation are shown in Fig. 1.5. Although the condition $\Gamma > 1$ is not necessary for pattern formation ([20], [21]), experimental observations revealed the onset of pattern formation for $\Gamma \gtrsim 4$. These waves were reproduced in quantitative agreement with numerical MD simulations by [22], [23], [24] and they were also found from a linear stability analysis of an oscillating granular layer, modeled as an isothermal incompressible fluid with vanishing surface tension [25].

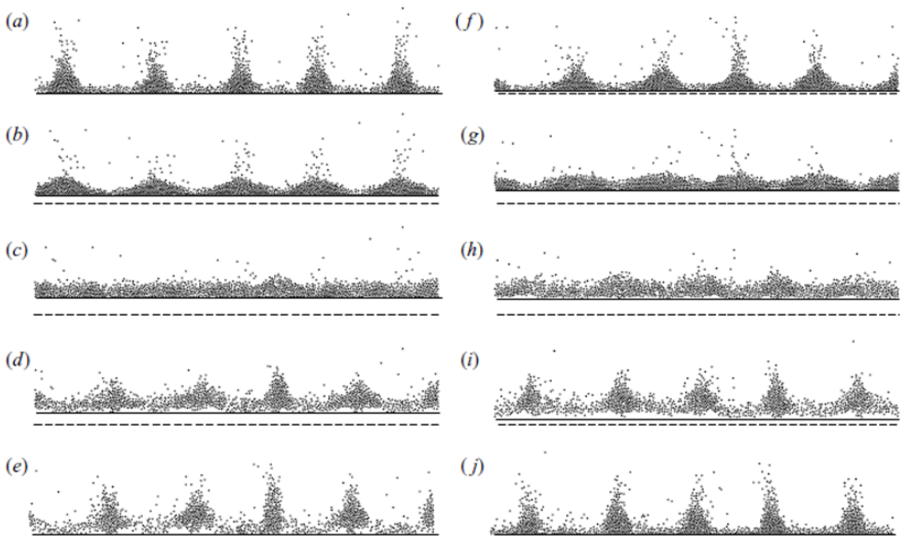

Figure 1.5: Periodic wave-like pattern in a vertically vibrated granular layer. The period of the pattern is twice the period of the excitation. This figure shows a two-dimensional MD simulation of 3000 particles at $A = 4.02$, $f = 3.5$ ($\Gamma = 0.197$). The dashed line indicates the lower amplitude of the oscillation. (Figure from [19]).

Recently, Eshuis *et. al.* [7] found undulation patterns on a vibrated granular bed held in a quasi two-dimensional (2D) rectangular Perspex® container as shown in Fig. 1.6. *Undulations* or *"ripples"* or *"arches"* are a type of standing waves whose time period of oscillations are twice the time period of shaking; this is the reason they are referred as $f/2$ *waves*.

Oscillons: Oscillons are stable two-dimensional localised excitations which have the tendency to assemble into "molecular" and "crystalline" structures. These oscillons were discovered by Umbanhowar *et. al.* [18] in a shallow vibrating layer of sand. These are formed when a shallow granular layer is vertically vibrated by sinusoidal excitaion given by eqn. (1.1).

Oscillons are small, circularly symmetric excitations which oscillate at a frequency $f/2$: during one cycle it is a peak; and on the next cycle it is a crater (Fig. 1.7). The diameter of oscillons depends on Γ but is typically 30 particles (4% of the container diameter). Oscillons form with equal probability at all locations within the plane of the layer and often persist for more than 5×10^5 conatiner oscillations. They do not propogate but they do drift slowly and randomly, taking about 10^3 cycles to move a distance equal to their diameter [18]. Oscillons of like phase show

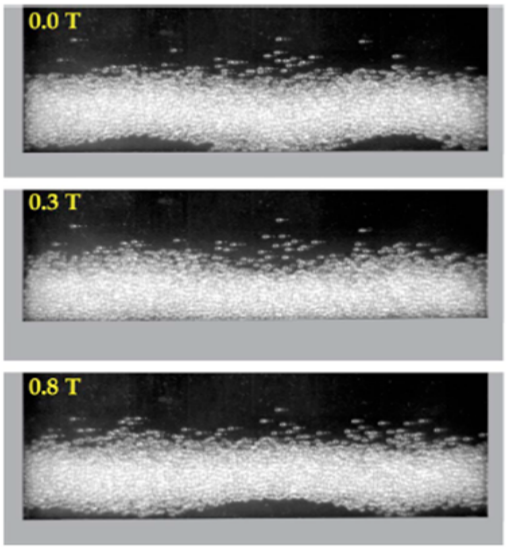

Figure 1.6: One complete standing wave cycle of the $n = 4$ undulation mode for $F = 9.4$ particle layers at $\Gamma = 12$ ($A = 2.0\ mm, f = 39.3\ Hz$), as observed by Eshuis *et. al.* in their experiments (taken from [7]).

a short range, repulsive interaction, while oscillons of opposite phase attract and bind. When a peak and a crater collide they attract each other and form a stable dipole structure, see Fig. 1.8 (a) and (b). Other stable combinations of peak and crater exists for which the constituent oscillons have coordination number greater than one, see Figs. 1.8 (c) and (d). Triangular tetramer structures also form in which the central oscillon has coordination number three, see Figs. 1.8 (e) and (f). Small oscillons may separate from the lattice and then disappear, see Fig. 1.8 (g).

Hexagonal Patterns

Planar patterns have also been reported by Umbanhowar *et. al.* [18] in experiments with a two-frequency forcing:

$$y = A\sin(2\pi f_1 t) + B\sin(2\pi f_2 t + \pi/2). \tag{1.2}$$

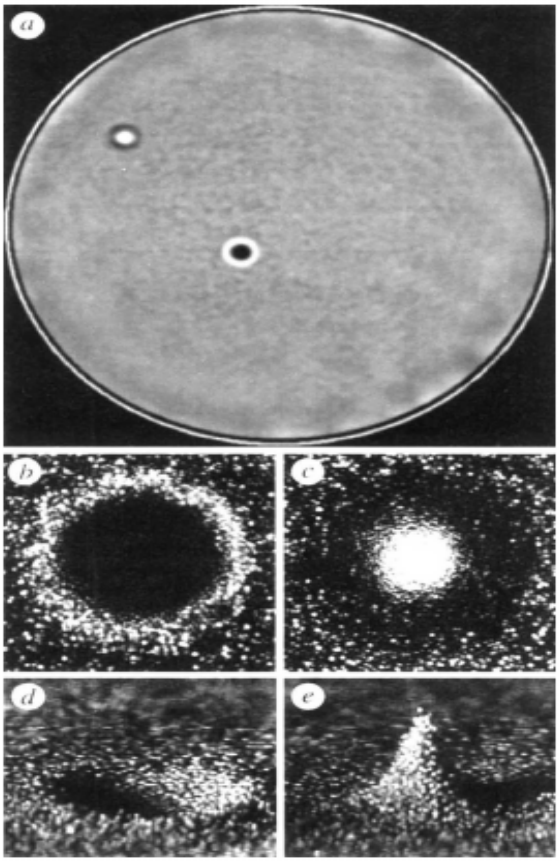

Figure 1.7: Two oscillons with opposite phase. (b) and (c), A single oscillon viewed from above, at times differing by $1/f$. (d) and (e), Corresponding side views ($f = 26\ Hz$, $\Gamma = 2.45$, layer depth of 17 particles). The individual particles (0.15-0.18 mm diameter bronze spheres) are in close contact, as can be seen in (b)-(e), which show 7 $mm \times 7$ mm regions of the 127 mm diameter container. Vaccuum of 0.1 torr is created inside the container (taken from [18]).

When Γ is decreased into the oscillon region, the hexagonal pattern becomes a hexagonal crystal of oscillons with the same phase, see Fig. 1.9(a). These oscillons are weakly repelling and hence do not bind together. When Γ is increased from this oscillon state, these oscillons expand to form a cellular honeycomb pattern, see Fig. 1.9(b) and Fig. 1.9(c).

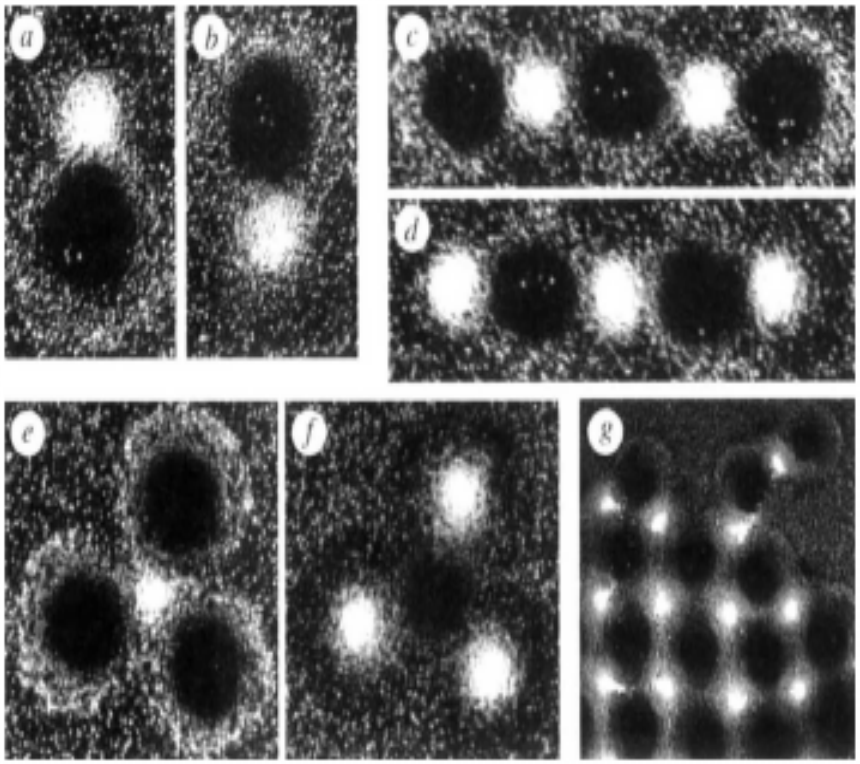

Figure 1.8: Oscillon 'molecules' and 'crystal': (a),(b), dipole; (c),(d), polymeric chain; (e),(f), triangular tetramer; (g), square ionic lattice. The pairs of pictures in (a)-(f) are separated in time by $1/f$. In all pictures the separation between adjacent oscillons of opposite phase is approximately 4 mm. In (g), a small chain separates from the edge of the square lattice (taken from [18]).

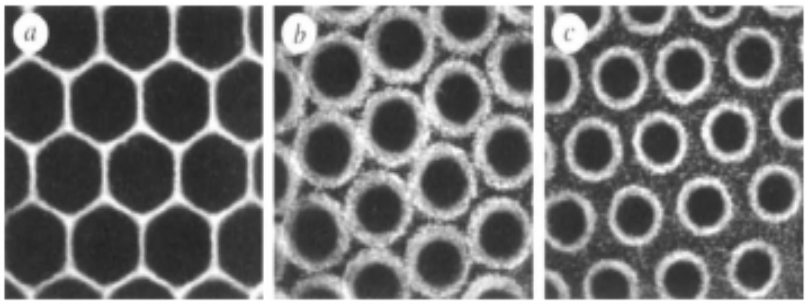

Figure 1.9: Hexagonal patterns with two-frequency forcing, $y = A\sin(2\pi f_1 t) + B\sin(2\pi f_2 t + \pi/2)$ with $B/A = 0.04$, $f_1 = 26\ Hz$, and $f_2 = 13\ Hz$. (a) Above the planar pattern threshold ($\Gamma = 2.7$), (b), at the threshold ($\Gamma = 2.50$), and (c) below the threshold($\Gamma = 2.45$). Each frame is $40 \times 40\ mm$ (taken from [18]).

Square & Stripe Patterns: Umbanhowar *et. al.* [14] experimentally observed square and stripe patterns in a thin layer of grains filled in a "square shaped" container, see Fig. 1.10.

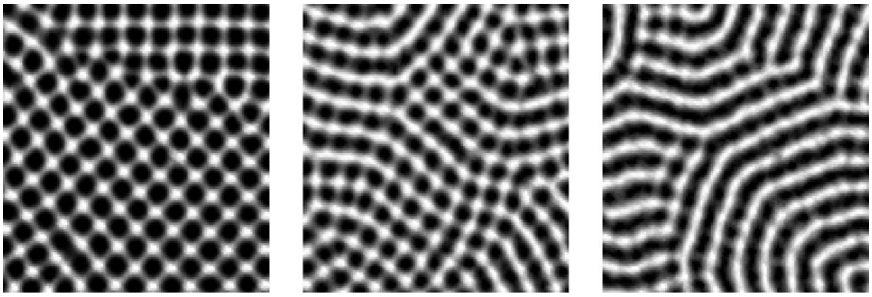

Figure 1.10: Images of granular wave patterns near onset: (left) squares, $f = 33\ Hz$ ($f^* = 0.28$), (center) squares and stripes, $f = 37\ Hz$ ($f^* = 0.31$), and (right) stripes, $f = 43\ Hz$ ($f^* = 0.36$). In each case bronze grains of diameter 1.0 mm are held in a square shape container with $N = 4$, $\Gamma = 2.5$ and the image size is $40.5 \times 40.5\ mm$.(Figure from [14]).

Three dimensionless control parameters used in the experiments of Umbanhowar *et. al.* [14] are: the dimensionless acceleration $\Gamma = A/omega^2/g$, the scaled frequency $f^* = f\sqrt{H/g}$, and the layer thickness $N = H/D$. All the above patterns are marked in a phase diagram in the (Γ, F)-plane as shown in Fig. 1.11.

1.2.2 Scaling Relations for wavelengths of Standing Waves

The dependence of the wavelength λ on frequency f for standing waves is given by

$$\lambda = \lambda_{min} + g_{eff}/f^2, \tag{1.3}$$

as found by Melo *et. al.* [8], Clément *et. al.* [10], and Metcalf *et. al.* [11] in experiments. The deviation from this dispersion relation at higher frequencies, which is related to the minimum wavelength, is due to the finiteness of the particle. Alternativley, Clément *et. al.* [10] suggested a dispersion relation

$$\lambda/\sqrt{N} = \lambda^*(d) + g^*/f^2, \tag{1.4}$$

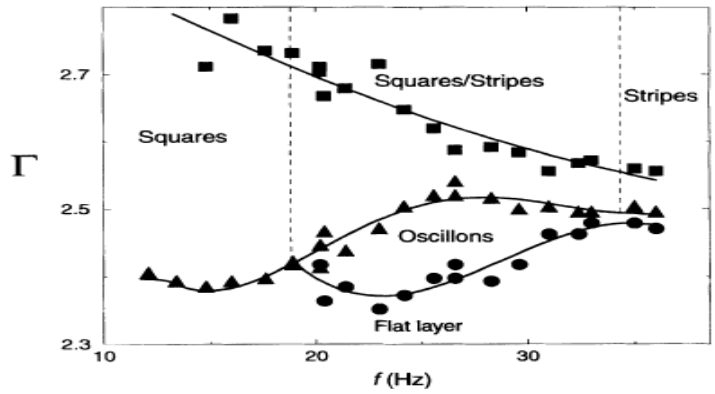

Figure 1.11: Diagram showing the stability regions for different states, as a function of f and Γ, for increasing Γ (squares) and decreasing Γ (triangles and circles). The transitions from the flat layer to squares and stripes are hysteretic, but the hysteresis is much smaller for stripes. Oscillons are observed for layers greater than 13 particles deep in a range of f which increases with increasing depth (taken from [18]).

where $\lambda^* = 7.2\ mm$, $g^* = 1.05\ m/s^2$. Bizon *et. al.* [16] and Umbanhowar *et. al.* [14] suggested a scaling using layer height, i.e. $\lambda^* = \lambda/h$ and $f^* = f\sqrt{h/g}$. Recently, Sano *et. al.* [15] suggested

$$\frac{\lambda}{d} \propto \left(f\sqrt{\frac{d}{g}}\right)^{\alpha}, \tag{1.5}$$

where $\alpha \approx -2$ for lower frequencies and $\alpha \approx -2/3$ for higher frequencies. On the other hand, Umbanhowar and Swinney [14] found

$$\frac{\lambda}{h} \propto const + \left(f\sqrt{\frac{h}{g}}\right)^{\alpha} \tag{1.6}$$

where $\alpha = -1.32 \pm 0.03$.

1.3 Present Work: Vibrated Granular Bed

1.3.1 Present Work

The present thesis deals with an experimental study of vertically vibrated granular matter held in a quasi two-dimensional (2D) rectangular Perspex® container. Experiments are conducted on both monodisperse system (glass balls of diameter $d = 1.0\ mm$) and bidisperse mixtures. Two types of binary mixtures have been considered: (1) the glass and steel balls both having diameter of 1.0 mm and a density ratio of $\rho_g/\rho_s = 0.33$ and (2) the delrin and steel balls both having diameter of 1.0 mm and a density ratio of $\rho_d/\rho_s = 0.18$). We found various patterns in a shaken monodisperse system: spiked structures (f/4 ripples), undulations, granular Leidenfrost effect, convection rolls and the granular gas. The phenomena observed are similar in characteristics to the observations made in the experimental study by Eshuis *et. al.* [7], except the appearance of "f/4" ripples. We also found differnces with Eshuis *et. al.* [7] on the critical values of Γ for the onset of some patterns. In binary mixtures, we observed spiked structures, undulations, granular Leidenfrost effect, convection rolls and segregation. All the experiments are done by increasing the shaking intensity (measured in terms of dimensionless shaking acceleration Γ) while keeping the shaking amplitude A to be a constant. For a fixed number of particle layers, a gradual increase of the shaking intensity leads to transitions from one phenomena to another at a critical Γ value. The onset of various phenomena has been combined on $\Gamma - F$ plane to construct phase diagrams.

1.3.2 Organisation of Thesis

Chapter 2 This chapter deals with the description of experimental setup and the working principles of instruments used. The specifications of the electromagnetic shaker and the high speed camera have been discussed. After this the experimental procedure has been explained in detail.

Chapter 3 The chapter deals with the description of various phenomenon observed for a shaken monodisperse system of glass balls . The various phenomenon observed in the order in which they appear with increasing shaking streangth at constant shaking amplitude are bouncing bed, "f/4" ripples, undulations, granular Leidenfrost state, granular Convection and granular gas. This chapter concludes

with the construction of phase diagrams on (Γ, F)-plane or (S, F)-plane.

Chapter 4 In this chapter the experimental results on two types of binary granular mixtures have been discussed. Two types of bidisperse mixtures have been used: (1) glass and steel balls mixture both having diameters of 1.0 mm and a density ratio of $\rho_g/\rho_s = 0.33$ and (2) delrin and steel balls mixture both having diameters of 1.0 mm and a density ratio of $\rho_d/\rho_s = 0.18$. All the observed phenomena are combined on a phase diagram in (Γ, F)-plane.

Chapter 5 The experimental results have been summarised in this chapter.

CHAPTER 2

EXPERIMENTAL SETUP AND PROCEDURE

In this chapter, the experimental setup and experimental procedure have been discussed in detail. The electromagnetic shaker system and a high speed camera specification have been explained in following sections.

2.1 Experimental Setup

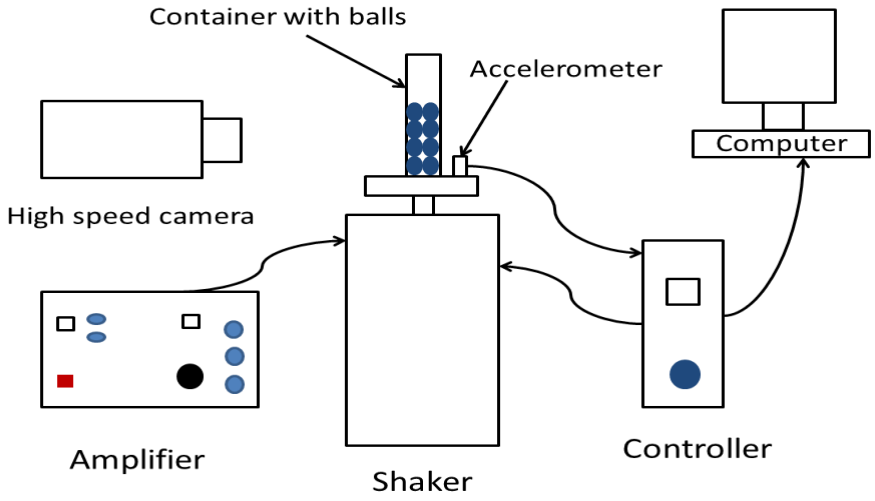

Figure 2.1: Sketch showing the experimental setup.

A sketch of the setup is shown in Fig. 2.1. The main part of this setup is a quasi two-dimensional container partially filled with spherical balls. The dimensions of the container are $L \times D \times H = 100 \times 5.5 \times 90\, mm$ (with L being the container length, D the depth, and H the height, see Fig. 2.2(d)). The container is subjected to vertical vibration by mounting it on an electromagnetic shaker. Spherical glass balls of diameter 1.0 mm have been used as granular materials. The experimental images have been recorded using a high speed camera at 1000 frames per second. Since the frame rate is high, a light source of very high intensity has been used to

get bright pictures within the short exposure time (of the order of one-tenth of a millisecond).

2.1.1 Shaker System

The picture of our electromagnetic shaker with the Heleshaw container is shown in Fig. 2.2. The main components of shaker system are: (1) electromagnetic shaker, (2) amplifier and (3)controller with a software interface (from Ling Dynamics System).

Specifications of Shaker:

- Shaker : Ling Dynamics System (Brüel & Kjær, Denmark),
- Type: Permanent magnet V456
- Moving armature mass: 0.43 kg
- Armature Diameter: 63.5 mm
- Useful frequency range: 5 - 7500 Hz
- System Sine Force Peak: Forced Air Cooled- 489 N
- Maximum Acceleration Sine Peak : 117 (g_n), where $g_n = A\omega^2/g$
- System Displacement Continuous (peak-peak) : 19 mm

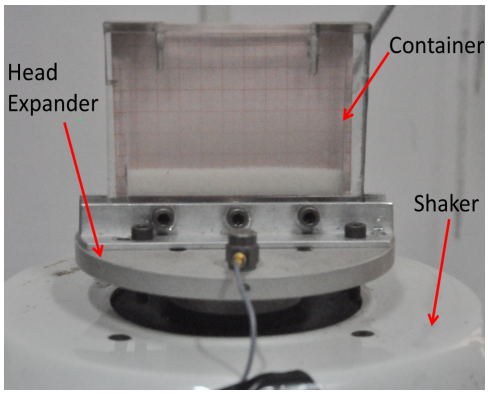

(a)

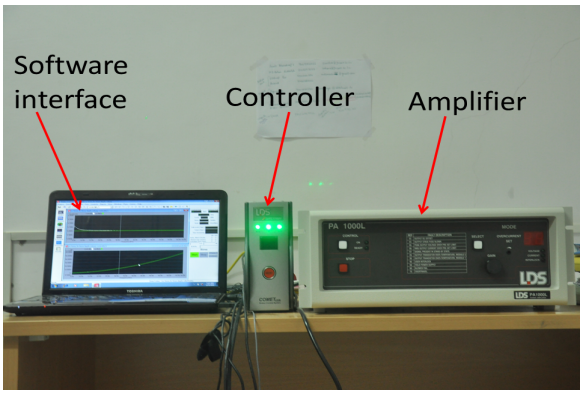

(b)

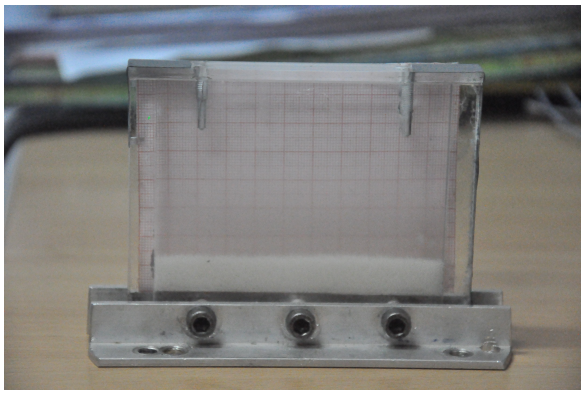

(c)

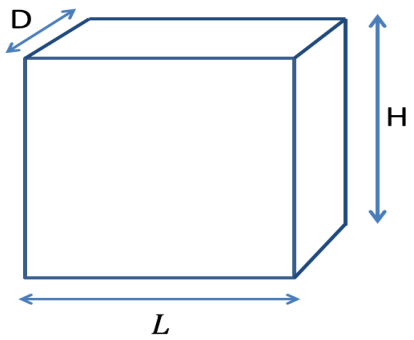

(d)

Figure 2.2: Shaker system: (a) Shaker holding container partially filled with balls, (b) Controller with amplifier, (c) Quasi two-dimensional (2D) Perspex® container, (d) Sketch of the container.

Specifications of Amplifier

- Power amplifier: Ling Dynamics System (Brüel & Kjær)
- Type: PA 1000L
- Amplifier rating: 1.4 KVA

Controller and Accelerometer :

- Controller: Brüel & Kjær(Denmark)
- Type: $COMET_{USB}$
- Accelerometer: DeltaTron®, Type: Piezoelectric 4513-001

2.1.2 Design of Container and Head Expander

Design of Container: The container is a quasi two-dimensional Heleshaw-type cell of dimensions $L \times D \times H = 100 \times 5.5 \times 90\, mm$ (with L being the container length, D the depth, and H the height) made of Perspex® sheet of 5 mm thickness, see Fig. 2.2(c) and Fig. 2.2(d).

The weight of the container with aluminium clamps and connecting screws is 334.8 gram.

Design of Head Expander: The container is mounted on a head expander fabricated from Aerospace Grade Magnesium Alloy. The design of the head expander is shown in Fig. 2.3.

The weight of the head expander with six connecting screws is 451 gram, and the total payload on the shaker is 800 gram.

2.1.3 Operating the Shaker System

The shaker operates on a "*closed loop*" system controlled by a controller with the amplifier through a Ling Dynamics System (LDS) software interface. To generate the feedback signal of required amplitude and frequency of the sinusoidal vibration, a piezoelectric accelerometer is mounted on the head expander. The software interface allows us to set two types of vibration profiles :

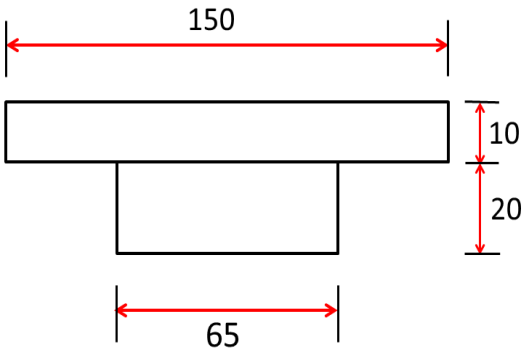

(a)

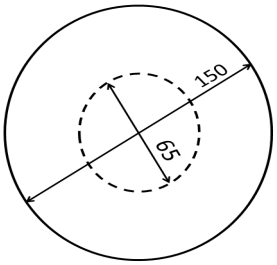

(b)

Figure 2.3: Design of head expander: (a) Front view, (b) Top view.

- "*Value Swept Sine software*" is used to set up a profile in which a range of frequency can be sweept at a constant shaking amplitude at any desirable sweep rate (linear as well as logarithmic). The frequency sweep rate in most of the experiments is 0.1 Hz/sec. We found this sweep rate to be optimal for observing all phase transitions in detail. The frequency sweeping can be performed both in the direction of increasing frequency and in the direction of decreasing frequency. The maximum frequency range (starting from a minimum frequency of 5 Hz) which can be swept at a constant amplitude A is limited by the maximum "g level"($\equiv \Gamma$) of the shaker and the peak sine force the shaker can achieve. The range of frequency depends on the constant shaking amplitude at which the shaker is required to be operated as shown in Fig. 2.4.

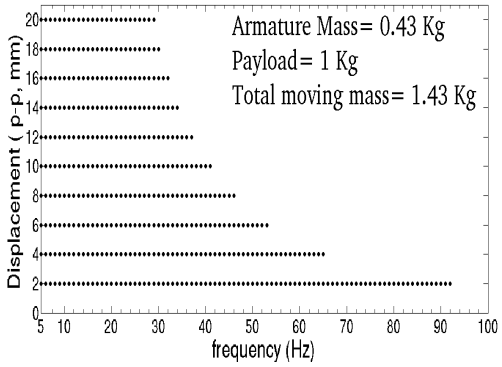

(a)

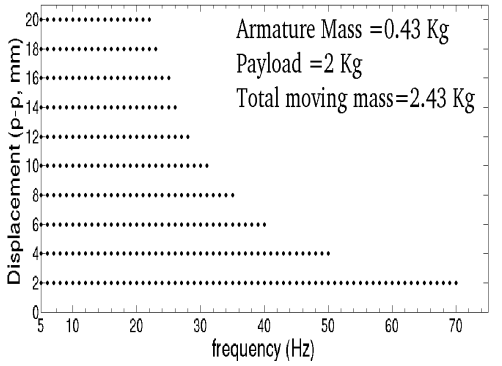

(b)

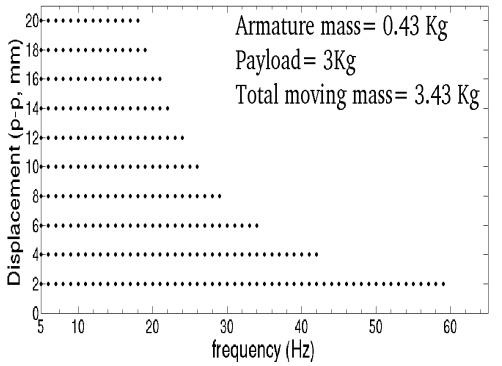

(c)

Figure 2.4: The maximum limit of frequency which can be achieved at a constant shaking amplitude with our shaker model (LDS-V456): (a) for a payload of 1 kg , (b) for a payload of 2 kg, and (c) for a payload of 3 kg.

- "*Sine Oscillator software*" is used to vary the shaking amplitude at a constant frequency. In this mode the shaker actually operates in an "*open loop*"

system where the accelerometer is used only to measure the amplitude level of shaking.

2.1.4 High Speed Camera

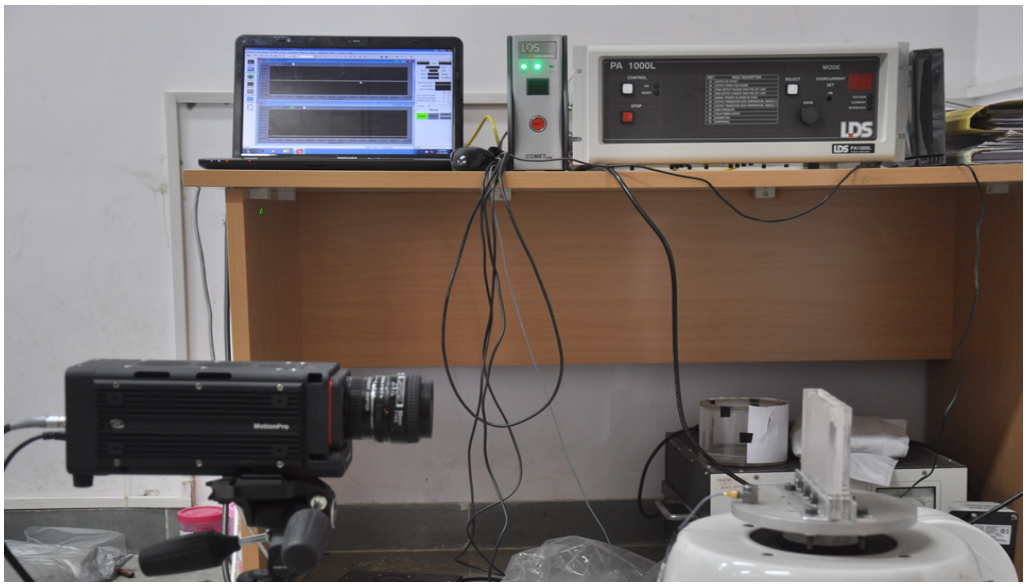

Figure 2.5: High Speed Camera used to capture experimental images

The specifications of our high speed camera are given below:

- Maximum frames per second (fps) @ Maximum Resolution: 5100 fps @ 1016× 1016
- Plus Mode: 9820 fps @ 1016 × 1016
- Memory 8 GB: 1.48 sec 7998 frames
- Maximum Frame Rate: 200000 fps @ 1016 × 16
- Minimum Exposure Time: 1 μs
- Sensitivity: 6000 ISO Mono, 2000 ISO Color
- Sensor Type: CMOS-Polaris II
- Sensor Size: 13.9 × 13.9 mm

- Array size: 1.0 mega pixel
- Pixel Size: $13.68 \times 13.68\ \mu m$
- Pixel Depth: 10 bit mono 30 bit color
- Mount: C-Mount standard
- Ethernet: 100/1000 BaseT
- USB 2.0: Standard

2.2 Experimental Procedure

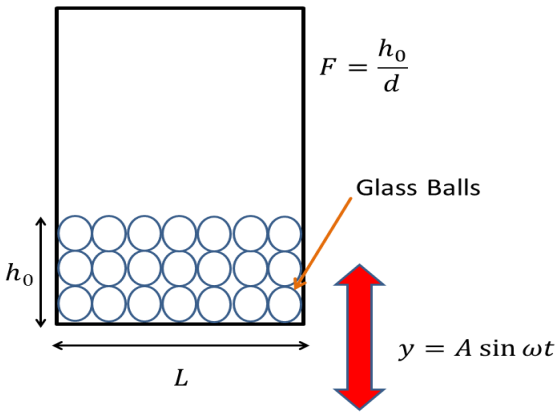

Figure 2.6: Sketch of vertically vibrated container holding monodisperse granular materials.

The container is subjected to a sinusoidal vibration produced by the shaker:

$$y = A \sin \omega t = A \sin(2\pi f t). \tag{2.1}$$

where A is the amplitude and f the frequency of shaking. During the experiments, the vibration intensity has been gradually increased by increasing the frequency while maintaining the shaking amplitude A to be constant. This type of frequency sweeping at a constant amplitude is achieved by the closed loop shaker system with the help of a software. The dimensionless control parameters used to analyze the experiments are:

- The dimensionless shaking accelaration:

$$\Gamma = \frac{A\omega^2}{g}. \tag{2.2}$$

where A is the shaking amplitude, $\omega = 2\pi f$ with f being the frequency and g is the acceleration due to gravity.

- Another shaking parameter can be constructed as:

$$S = \frac{A^2\omega^2}{gd} = \Gamma\left(\frac{A}{d}\right). \tag{2.3}$$

Eshuis *et. al.* [7] showed that the shaking strength "S" is more appropriate to construct phase diagrams for strong shakings.

- **Number of ball layers at rest** F. In the experiments the number of layers are varied from 3 to 14.

$$F = \frac{h_0}{d}, \tag{2.4}$$

where h_0 is the bed height at rest, see Fig. 2.6. The number of layer in our experiments has been been varied from 3 to 16.

- **Aspect ratio** (see Fig. 2.6)

$$L/h_0 \tag{2.5}$$

The aspect ratio is varied by changing the bed height (i.e. by changing the number of layers F). The aspect ratio in our experiments is very large ($L/h_0 >> 1$).

2.3 Specifications of spherical particles

The particles used in our experiments are monodisperse, and thier specifications are given below. These precision balls were imported from Italy (R.G.P. International, Cinisello Balsamo, Italy).

2.3.1 Soda Lime Glass Balls

- Diameter: 1.0 mm

- Grade 500
- Sphericity Tolerance: 10 μm
- Specific Weight: 2500 kg/m^3

2.3.2 Steel Balls

- Diameter: 1.0 mm
- Grade 10
- Sphericity tolerance: 0.25 μm
- Specific Weight: 7650 kg/m^3

2.3.3 Delrin Balls

- Diameter: 1.0 mm
- Grade I
- Sphericity tolerance: 12 μm
- Specific Weight: 1420 kg/m^3

CHAPTER 3

RESULTS FOR MONODISPERSE SYSTEM

In this chapter, the experimental results of vertically vibrated monodisperse granular materials are discussed and summarized in the form of phase diagrams. The monodisperse system comprises of glass balls of diameter $d = 1.0\ mm$ held in a rectangular quasi two-dimensional (2D) setup, see Fig. 3.1. The experiments have been performed by increasing shaking intensity ($\Gamma = A\omega^2/g$) via upsweeping frequency at three constant shaking amplitudes ($A = 2.0\ mm$, $A = 3.0\ mm$ and $A = 4.0\ mm$). The frequency sweep rate is linear ($0.1Hz/sec$). Various phenomena observed with increasing shaking strength are reported. The control parameters are as follows:

- Dimensionless shaking acceleration: $\Gamma = \dfrac{A\omega^2}{g}$
- Number of layers at rest: $F = \dfrac{h_0}{d}$
- Shaking amplitude: $\dfrac{A}{d}$

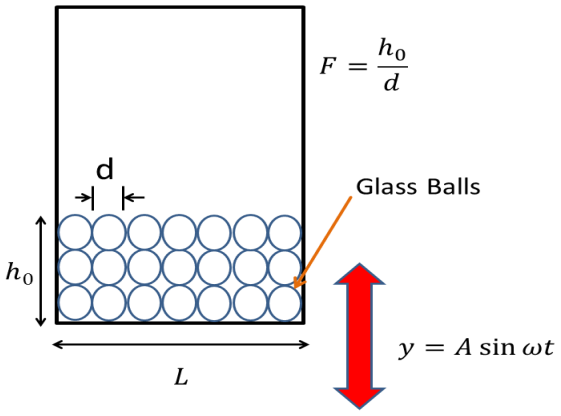

Figure 3.1: Sketch of vertically vibrated container holding monodisperse granular materials.

3.1 Heaping and Deheaping Phenomena

As we gradually increase the dimensionless shaking acceleration Γ by increasing frequency f (starting from a minimum frequency of 5 Hz) at a constant shaking amplitude (A), the onset of heaping takes place and on further increasing this Γ-level, the bouncing bed (see section 3.2) has been observed. In the heaping phenomenon the bed forms a heap on left side of the container and then gets levelled up (deheaping) as the bed starts bouncing, see Fig. 3.2. It should be noted that the onset of heaping (Γ_{heap}) occurs before the onset of bouncing bed phenomenon (see section 3.2) and it further continues even in the bouncing bed regime for a small range of Γ.

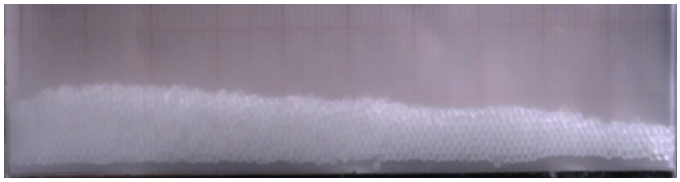

(a) t=0.0T

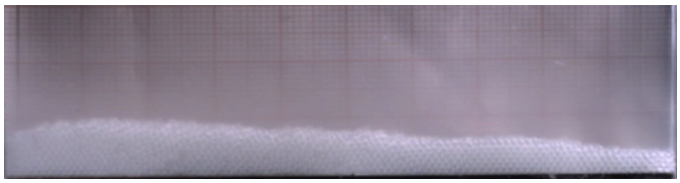

(b) t=0.25T

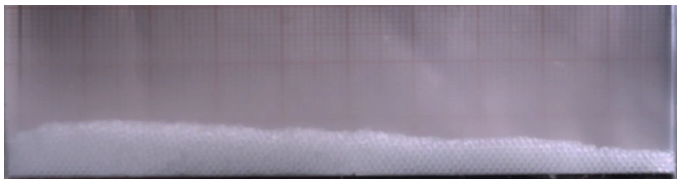

(c) t=0.5T

Figure 3.2: Snapshots of the heaping phenomena on the left side of container at successive time instants of the cycle for $F = 9$ layers of $d = 1.0\ mm$ glass beads at shaking acceleration $\Gamma = 1.7$ ($A = 4.0\ mm, f = 10.28\ Hz$). T= $1/f$ is the time period of shaking $y = A\sin(2\pi ft)$.

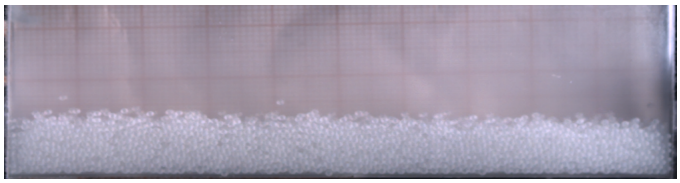

(a) t=0.0T

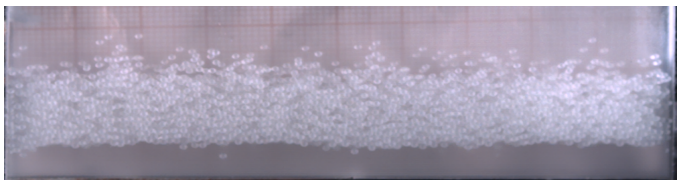

(b) t=0.5T

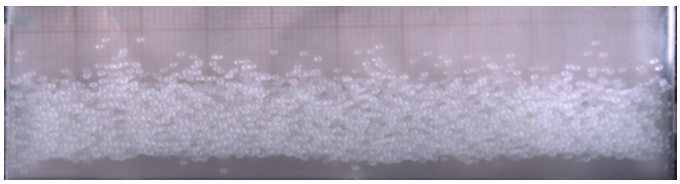

(c) t=0.6T

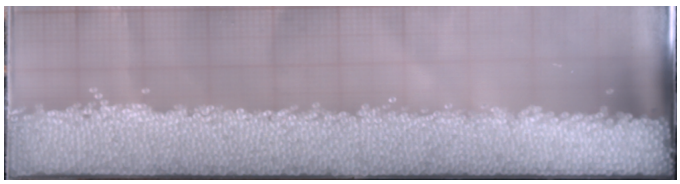

(d) t=T

Figure 3.3: Snapshots of the bouncing bed at successive time instants of the cycle for $F = 9$ layers of $d = 1.0\ mm$ glass beads at shaking acceleration $\Gamma = 3.62$ ($A = 4.0\ mm, f = 15Hz$). T$= 1/f$ is the time period of shaking $y = A\sin(2\pi ft)$.

3.2 Bouncing Bed

For shaking accelerations $\Gamma \sim 1$, the granular bed behaves like a solid, comoving with the container base without detaching from it. To detach the bed from the vibrating base, at some point of oscillation cycle the base should have downward acceleration greater than gravity plus the friction between the bed and the walls of the container. In this case the bed bounces in a similar way as a single particle bouncing off a plate, and therefore it is called *bounicng bed*, see Fig. 3.3. The value of Γ corresponding to the onset of bouncing bed is determined by gradually increasing frequency f at a constant amplitude. This onset value of Γ increases

with the number of layers F as shown in Fig. 3.4. The explanation for this [7] lies in the fact that with increasing number of layers, the contact area with the side and front walls of the container increases which in turn proportionally increases the frictional force, leading to a higher value of Γ_{detach} for larger F. The average value of Γ_{detach} is fitted well by a power law:

$$\Gamma_{detach} = 1.277F^{\delta}, \qquad with \quad \delta = 0.1359. \tag{3.1}$$

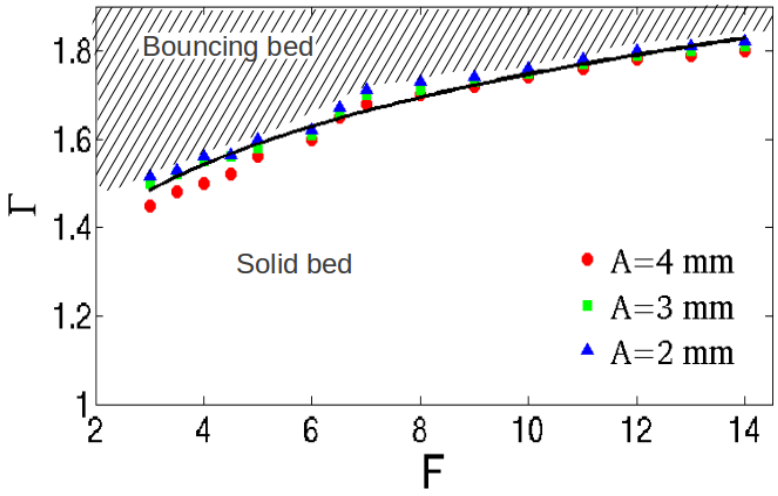

Figure 3.4: The transition from solid to bouncing bed is governed by dimensionless shaking acceleration Γ. The critical value of Γ increases with the number of particle layers.

3.3 Spikes (f/4 Ripples)

The wavy pattern formation in a granular layer due to vertical vibration has been studied experimentally [10], [17], [26], [7] as well as numerically [19], [22], [23], [24]. In our experimental study the surface instability in the form of an array of peaked structures and standing waves pattern (undulations) have been observed. The peaked structures are also called "spikes", see Fig. 3.5. These peaked structures are separated by a typical wavelength λ and a maximum peak height a [10], [17],

see Fig. 3.5.

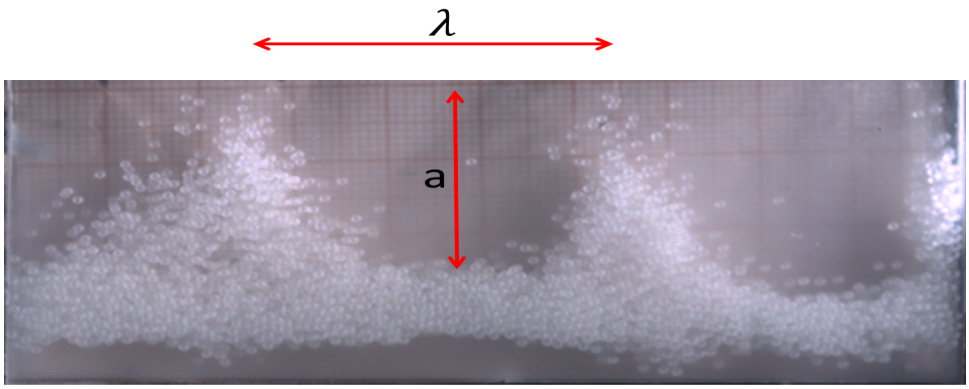

Figure 3.5: Snapshot of "f/4" ripples for $F = 9$ layers of $d = 1.0\ mm$ glass balls at shaking acceleration $\Gamma = 8.5$ ($A = 4.0\ mm$ and $f = 23Hz$).

Since it takes exactly four shaking periods to complete one full oscillation of these peaked structures these are called "$f/4$ ripples", see Fig. 3.6. The following features of these structures have been observed:

- During the "free" flight (ignoring boundary contacts) of the granular bed, the amplitude of the peaks grows until the base of the container hits the bed, see Fig. 3.6(c).
- The granular bed is carried in the upward direction by the base, relaxing the peak amplitude.
- The maxima position (peak) exchanges with the minima (valley) in every two shaking periods (see Fig. 3.6).

In our experiments the spikes ("f/4" ripples) emerged from the bouncing bed regime by gradually increasing dimensionless shaking acceleration (Γ) at a constant shaking apmlitude A as shown in Fig. 3.7. We observed spikes at two constant shaking amplitudes $A = 3.0\ mm$ and $A = 4.0\ mm$ whereas at $A = 2.0\ mm$ it was not observed. It is seen from Fig. 3.7(a) and 3.7(b) that the Γ-value for the onset of spikes at a constant shaking amplitude of $A = 3.0\ mm$ remains almost constant with increasing number of layers F but at $A = 4.0\ mm$ there is a slight variation.

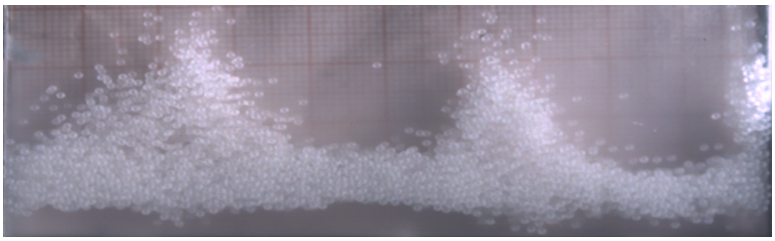

(a) t=0T

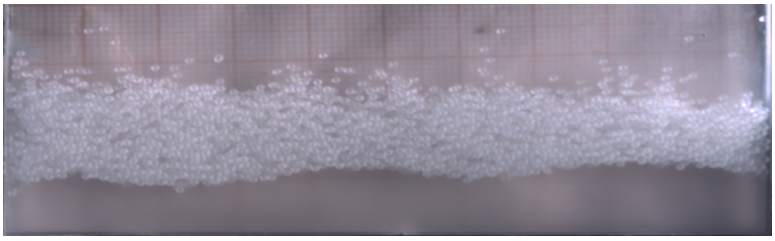

(b) t=T

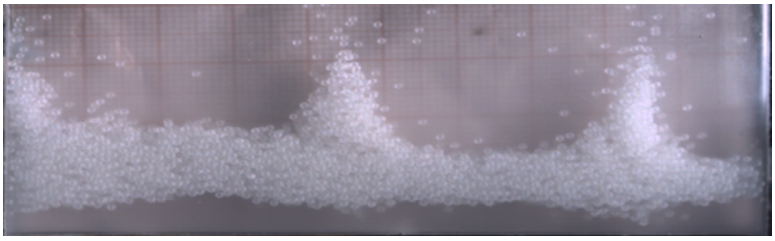

(c) t=2T

Figure 3.6: Snapshots of "f/4" ripples showing exchange of maxima (peak) and minima (valley) in two shaking periods for $F = 9$ layers of glass balls ($d = 1.0\ mm$) at $\Gamma = 8.5$ ($A = 4.0\ mm$ and $f = 23Hz$). T=$1/f$ is the time period of shaking $y = a\sin(2\pi ft)$.

For both shaking amplitudes, the onset of spikes from the bouncing bed occurs at $\Gamma \approx 7.0$, see Fig. 3.7(c).

3.4 Undulations

The undulations are standing wave patterns exhibited by the granular bed similar to a vibrating string (see Fig. 3.8). The *undulations* or *"ripples"* or *"arches"* are standing waves whose time periods of oscillation are twice the time period of shaking- this is the reason they are also called $f/2$ *waves* [7], [26], [8]. The undulation pattern takes one vibration cycle to exchange maxima and minima

positions (see Fig. 3.9).

The wavelength λ of the undulation pattern, such as that in Fig. 3.8, is given by

$$L = n\frac{\lambda}{2}, \qquad n = 1, 2, 3, ..., \tag{3.2}$$

where n is an integer number of half wavelengths of undulation that is accomodated in a container of length L.

Figure 3.10 shows the onset of successive undulation modes for different number of layers F. The mode number n increases with increasing dimensionless acceleration Γ.

If the shaking acceleration (Γ) is increased gradually, the undulation pattern evolves either from the bouncing bed regime or spikes depending on the number of layers (F) and shaking amplitude (A) as follows:

- At $A = 2.0\ mm$, the bouncing bed undergoes a transition directly to the gaseous phase for ($F \leq 4$) and for $F \geq 4.5$ the bed develops standing wave patterns known as *undulations* (see Fig. 3.8).

- At $A = 3.0\ mm$ and for $F \leq 3$, the bouncing bed transitions directly to gaseous phase; for $3.5 \leq F \leq 7$ the bed transitions directly to undulation regime and for $F \geq 8$ the bed first shows spikes (f/4 ripples, see Fig. 3.5) and then transitions to undulation regime.

- At $A = 4.0\ mm$ and for $F \leq 3$ the bouncing bed transitions directly to gaseous phase; for $3.5 \leq F \leq 6.5$ the bed transitions to undulation regime and for $F \geq 7$ the bed first shows spikes and then transitions to undulation regime.

Fig. 3.11 shows the onset values of Γ from bouncing bed to undulation waves for three amplitudes $A = 2.0, 3.0$ and $4.0\ mm$. It is observed that $\Gamma_{undulation}$ increases with increasing F for $F \leq 8$ and then saturates to a constant value of $\Gamma = 9.2$ for $F \geq 8$.

3.4.1 Theory for Undulatory Pattern

When the bed of particles collides with the vibrating base of the container, it is subjected to horizontal dilatancy [26], which causes the dilation of the string of

particles in contact with the base. If this dilation crosses a certain threshold level, it will give rise to buckling of the string and the particles start following an arch shape. Let s denote the position along the contour of the undulation, and $\theta(s)$ be the angle which the bed makes with the horizontal at any position s as shown in Fig. 3.12; the equation for $\theta(s)$ is given by [26]

$$\frac{d^2\theta}{ds^2} = -\alpha^2 \sin\theta, \tag{3.3}$$

where $\alpha = \sqrt{R/EI}$, with R being the reaction force from the side walls on the bed, E the effective Young's modulus of the bed, I its moment of inertia. In small angle approximation [7] $\sin\theta \approx \theta$, the above eqn. transforms to harmonic oscillator equation:

$$\frac{d^2\theta}{ds^2} = -\alpha^2\theta. \tag{3.4}$$

It is evident from Fig. 3.9 that the undulation mode is perpendicular to the side walls, we can put the boundary condition $\theta(0) = 0$ and $\theta(L) = 0$ to solve eqn.(3.3). The solution is $\theta = C_1\cos(\alpha s) + C_2\sin(\alpha s)$, where C_1 and C_2 are constants. Using boundary conditions, we get $\alpha = \dfrac{n\pi}{L}$ and θ is given by

$$\theta(s) = C_2 \sin\left(\frac{n\pi s}{L}\right). \tag{3.5}$$

Now, in small angle approximation $s \approx x$, i.e. the distance along the arc contour is approximately equal to horizontal distance. The vertical position of any point on the center of mass of undulation wave is given by

$$y = C_2\left(\frac{L}{n\pi}\right)\left[1 - \cos\left(\frac{n\pi x}{L}\right)\right], \quad n = 1, 2, 3.... \tag{3.6}$$

The undulation profiles obtained in experiments as shown in Fig. 3.13 qualitatively agree with the profiles generated by eqn. (3.7) (see Fig. 3.14). Figure 3.13 shows six successive undulation modes observed with increasing frequency for $F = 12$ layers of glass beads and $A/d = 2$.

3.4.2 Dispersion Relation for Undulation Waves

For showing the dependence of wavelength λ on the frequency of excitation various dispersion relations have been suggested in literature. Sano *et. al.* [15] suggested

$$\frac{\lambda}{d} \propto \left(f\sqrt{\frac{d}{g}} \right)^{\alpha}, \tag{3.7}$$

where $\alpha \approx -2$ for lower frequencies but $\alpha \approx -2/3$ for higher frequencies; d is the diameter of the particle. Umbanhower and Swinney [14] suggested

$$\frac{\lambda}{h} \propto C + \left(f\sqrt{\frac{h}{g}} \right)^{\alpha}, \tag{3.8}$$

where $\alpha = -1.32 \pm 0.03$ and h is the layer height. From our experimental data for undulation modes at different layer heights h with their onset at corresponding frequencies, a plot has been obtained (see Fig. 3.15). The ordinate shows the wavelength normalized with layer height $\lambda^* = \lambda/h$, whereas the abscissa is the normalized frequency $f^* = f\sqrt{h/g}$. The data points are best fitted by the relation:

$$\log \lambda^* = -1.8 \log f^* + 8.3. \tag{3.9}$$

Note that there is too much scatter in data. The exponent for the dispersion relation is $\alpha = -1.8$ which is close to that obtained by Sano *et. al.* for low frequency regime.

3.5 Granular Leidenfrost State

3.5.1 Original Leidenfrost State

This effect was first reported by Hermann Boerhaave in 1732 but thoroughly investigated by Johann Gottlob Leidenfrost in 1766 [28]. When a water drop impinges on a hot metal surface that is much hotter than the boiling point of water, the drop does not vaporize immediately but instead survives for astonishingly longer time hovering over its own vapor layer (see Fig. 3.16). This is known as Leidenfrost effect.

When the temperature of the hot surface is less than the Leidenfrost temperature (Leidenfrost temperature is above the boiling point of the liquid-droplet), the drop spreads over the surface and rapidly conducts heat through it, resulting in complete vaporization within a short time [29]. When the temperature of the surface is above the Leidenfrost temperature, the bottom surface of the drop which is in contact with the surface vaporizes immediately and due to the gas pressure of this vapor layer the rest of the drop floats on the surface, as shown in Fig. 3.16(a). This vapor layer slows down the rate of heat transfer (since water vapor is a poor conductor of heat) from the hot surface to the drop and hence the drop survives for quite a long time, as shown in Fig. 3.16(b) [29].

3.5.2 Granular Leidenfrost State

In granular Leidenfrost effect a dense cloud of particles is elevated and supported by a dilute gaseous region of fast moving particles below it [7] very much similar to the drop hovering on a hot surface over its own vapor layer. This was discovered by Eshuis *et. al.* [30].

Similar to experiments of Eshuis *et. al.* we observed Leidenfrost state originating from the undulation regime. When the highest undulation mode becomes unstable it vaporises to the gaseous state and a dense cluster of particles float over it as shown in snapshots in Fig 3.17. It should be noted in Fig. 3.17 that the coarse-grained density profiles undergo changes during an oscillation cycle. Figure 3.18 shows transition from undulation regime to the Leidenfrost state for three values of shaking amplitudes ($A = 2.0, 3.0$ and $4.0\ mm$) in the $(\Gamma - F)$-plane.

3.6 Granular Convection

When the shaking acceleration Γ is increased above a certain threshold value there is an onset of convection in the form of rolls (see Fig. 3.19). This is very similar to the formation of Rayleigh-Bénard convection rolls in a classical fluid heated from below , where the onset of instability in fluid motion is governed by the Rayleigh number which is the ratio of buoyancy force to the dissipative force [31], [32], [33].

Granular convection has been extensively studied experimentally [34] - [40], numerically [41]- [48] and theoretically [49]- [53]. These studies dealt with mild fluidization for which convection is nearly boundary driven but the convection we observed occurs at strong fluidization ($\Gamma > 25$) and shows large density differences, similar to Eshuis *et. al.* [7].

The mechanism behind the formation of convection rolls is as follows: there are some particles which have a higher granular temperature (excess energy above the mean kinetic energy) in comparison to sorrounding particles. These particles collectively move in the upward direction, and to balance this upward motion the neighbouring particles move downward, leading to the formation of convection rolls. In experiments it has been observed that the downward motion of particles initiates near the sidewalls and this is expected also because of the extra source for frictional dissipation provided by the side walls. Due to this reason, the first convection roll always emerges near one of the sidewalls. This first roll triggers formation of rolls throughout the entire container length, giving rise to a fully developed convection pattern (see Fig. 3.19). These convection rolls have similar characteristics as obtained previously in experiments by Eshuis *et. al.* [7]. When the shaking acceleration $\Gamma = a\omega^2/g$ is increased by increasing f or A, it has been noticed that the number of rolls in the convection pattern decreases (see Fig. 3.20). The reason is that as the vibration intensity increases, a larger amount of energy gets injected into the system because of which the rolls expand and a lesser number of rolls fits the container.

The transition to granular convection in our experiments has been observed from either the gaseous state or Leidenfrost State (see Fig. 3.19) depending on the number of layers F as follows:

- At constant shaking amplitude of $A = 2.0\ mm$, the transition to convection

occurs from the gaseous state for $3.5 \leq F \leq 4$ and from the Leidenfrost state for $F = 4.5$,

- At constant shaking amplitude of $A = 3.0\ mm$, the transition to convection occurs from the gaseous state for $3.5 \leq F \leq 4$ and from the Leidenfrost state for $4.5 \leq F \leq 6.5$,

- At constant shaking amplitude of $A = 4.0\ mm$, the transition to convection occurs from the gaseous state for $3.5 \leq F \leq 4.5$ and from the Leidenfrost state for $5 \leq F \leq 6.5$.

The above transitions are summarized in the Γ, F-plane in Fig. 3.21. One noteworthy difference with Eshuis *et. al.* [7] is that we found the transition to convection regime from both Leidenfrost state and gaseous state. In contrast, Eshuis *et. al.* [7] found this transition occuring from the Leidenfrost state as well as from the bouncing bed state.

3.7 Granular Gas

A collection of solid particles can be fluidized to a gaseous state by application of sufficiently strong forcing with $\Gamma >> 1$ [54]. In our experiments this granular gas has been realised by injecting the vibration energy into the system above a critical value (see Fig. 3.21). This state has been observed in other experiments and is well explained by hydrodynamic models [55], [56]. In a granular gas the particles interact by nearly instantaneous collisions (compared with the mean free time) in a way that is reminiscent of the classical picture of a molecular gas. This is the reason this fluidized phase of particles is known as a " granular gas " [57].

In spite of the similarity of a granular gas to that of a classical molecular gas, there are important differences between the two kinds of "gases." In a granular gas particle collisions are typically *inelastic* and this property plays a major role on the behavior of collections of particles. Figure 3.21 shows three snapshots of granular gas at various times of an oscillation cycle. The shaking acceleration in Fig. 3.21 is set to $\Gamma = 48.6$ and the number of layers is $F = 3$. The granular gas has been originated directly from the bouncing bed in this case. The granular gas state can also originate from the undulatory state when F is large as discussed in the next section.

3.8 Phase Diagrams : Comparison with Eshuis *et. al.*

Experimentally we have observed various phenomena occured in a vertically vibrated granular matter (spherical glass balls) as discussed above and identified the governing control parameters for each observed phenomena. Now we will discuss about the complete phase diagram in which we have represented all phenomena and their onset in Γ, F-plane for different shaking amplitudes ($A = 2.0\ mm, A = 3.0\ mm$ and $A = 4.0\ mm$). These phase diagrams are shown in Figs. 3.23(a), 3.23 (b) and 3.23(c).

The gradual increase of dimensionless shaking accleration Γ at a constant shaking amplitude A leads to a transition from solid to bouncing bed. For $\Gamma \sim 1$, the granular bed behaves like a solid comoving with the container base without detaching from it. If Γ is increased further, the bed starts bouncing just like a single particle does. The bouncing bed shows a transition to the gaseous regime, spikes (peaked structures) and undulations depending on the shaking amplitude and the number of particle layers. The size of the convection region in (Γ, F)-plane is smallest at $A/d = 2$, see Fig. 3.23(a).

3.8.1 Differences with Eshuis *et. al.*

We observed following differences with the previous work of Eshuis *et. al.* [30], [7], [58]:

- In our phase diagrams, for lesser number of particle layers F, we observed a transition to the convection regime from the gaseous phase whereas in phase diagrams of Eshuis *et. al.* such a transition was not observed. The phase diagrams of Eshuis *et. al.* are shown in Fig. 3.24.

- In phase diagrams of Eshuis *et. al.*, a transition to convection from bouncing bed has been observed whereas we did not observe such a transition from the bouncing bed. This can be ascertained by comparing Fig. 3.23 and Fig. 3.24.

- Our phase diagrams show spikes regime (f/4 ripples, see Fig. 3.5) for constant shaking amplitudes of $A = 3.0\ mm$ and $A = 4.0\ mm$. This spikes regime is sandwiched between the bouncing bed and the undulation regime, see Fig.

3.23(b) and Fig. 3.23(c). In contrast, the spikes regime is absent in phase diagrams of Eshuis *et. al.*, see Fig. 3.24.

- We also found the heaping and deheaping phenomena in our experiments (see Fig. 3.2). In the heaping phenomenon the bed forms a heap on left side of the container and then gets levelled up as the bed starts bouncing. This phenomenon was not observed by Eshuis *et. al.*

- The data points showing the onset of convection for shaking amplitudes $A = 2.0\ mm, 3.0\ mm$ and $4.0\ mm$ collapse better on (S-F) plane in case of Eshuis *et. al.*, see Fig. 3.23(a). However, in our case these data points do not collapse well (see Fig. 3.22b) in the (S-F) plane. Note that $S = \Gamma(A/d) = A^2\omega^2/gd$ is a measure of the mean kinetic energy injected into particles via the electromagentic shaker.

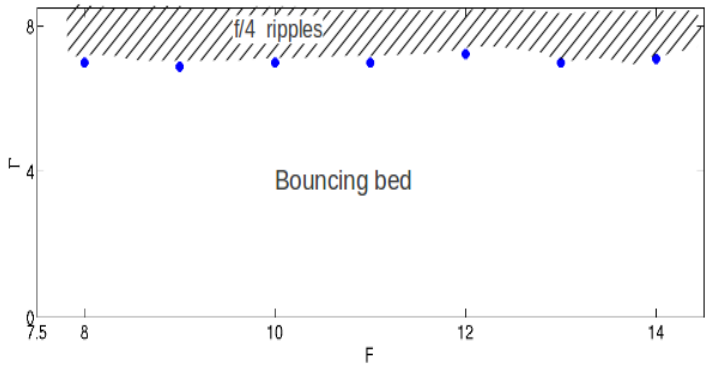

(a)

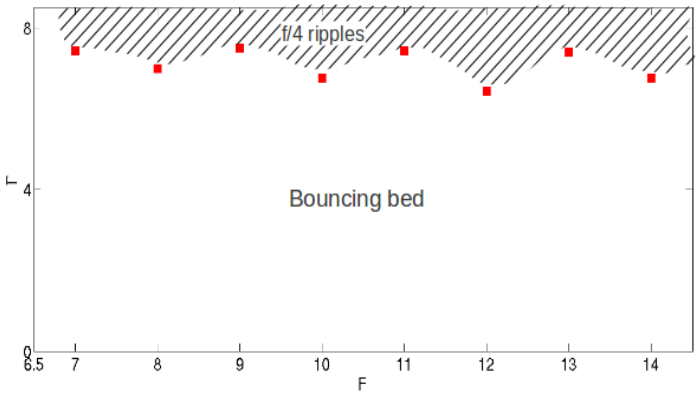

(b)

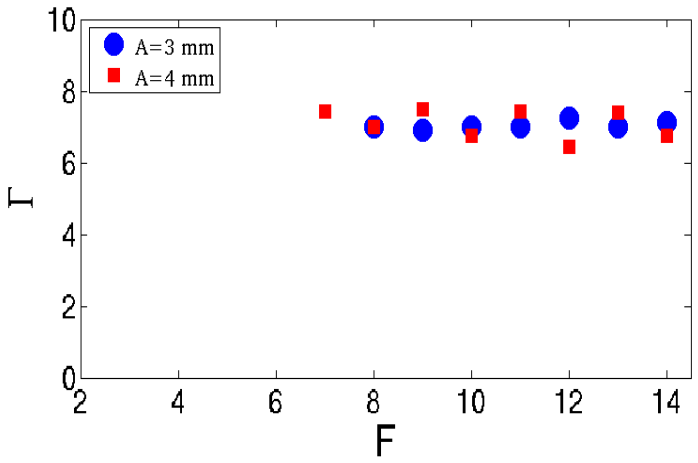

(c)

Figure 3.7: The transition from bouncing bed to spikes ("f/4" ripples) at two constant shaking amplitude (a) $A = 3.0\ mm$, (b) $A = 4.0\ mm$, (c) combined data for both shaking amplitudes.

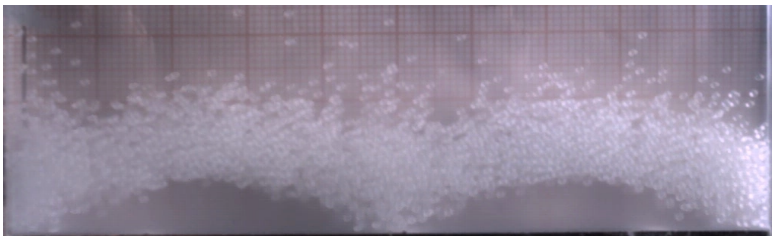

Figure 3.8: Snapshots of $n = 4$ undulation mode for $F = 7$ layers of $d = 1.0\ mm$ glass balls at shaking acceleration $\Gamma = 12.35$ $(A = 3.0\ mm, f = 32Hz)$. n is the integer number of half wavelengths that fits in the container.

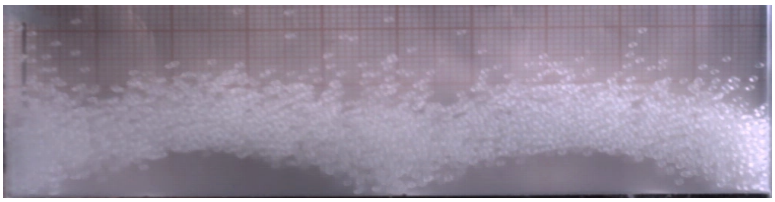

(a) t=0.0T

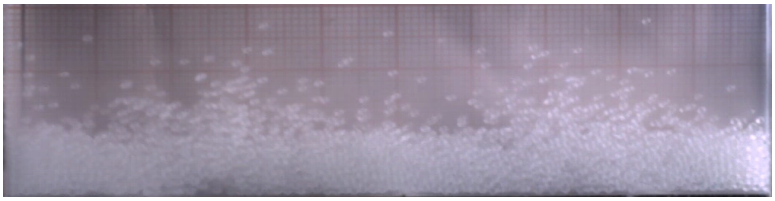

(b) t=0.48T

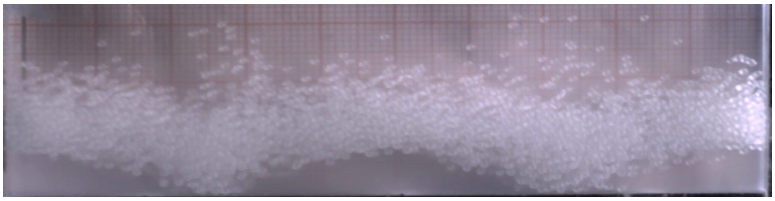

(c) t=T

Figure 3.9: Snapshots of one complete standing wave cycle of $n = 4$ undulation mode for $F = 7$ layers of $d = 1.0\ mm$ glass balls at shaking acceleration $\Gamma = 12.35$ $(A = 3.0\ mm, f = 32Hz)$. n is the integer number of half wavelengths that fits in the container.

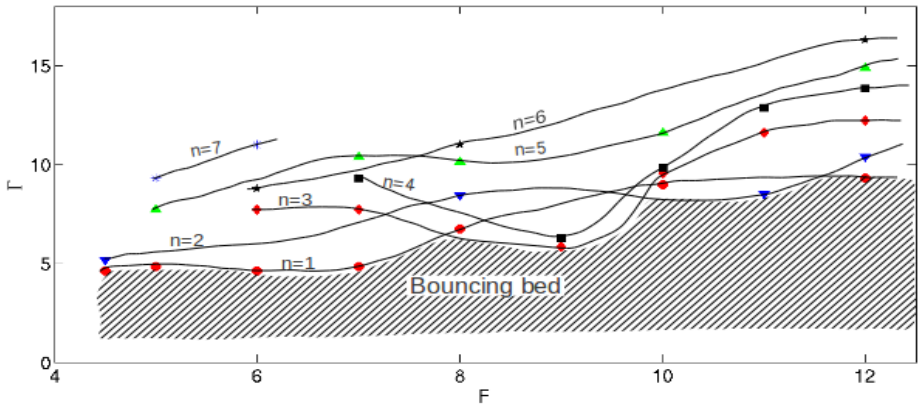

Figure 3.10: The onset of successive undulation modes $n = 1, 2, ..., 6$ in $\Gamma - F$ plane at a shaking amplitude $A = 2.0\ mm$. It is clear that the mode number increases with shaking acceleration.

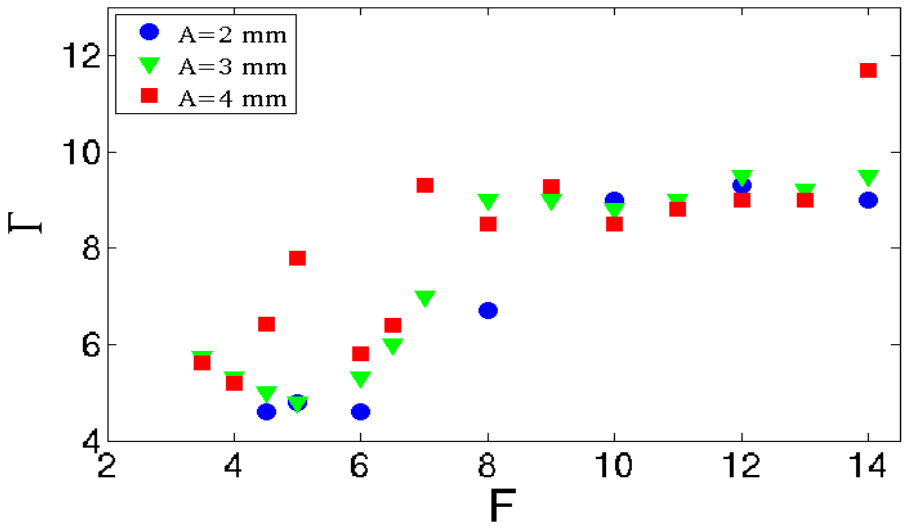

Figure 3.11: Onset values of Γ from bouncing bed to undulation waves for three shaking amplitudes $A = 2.0,\ 3.0$ and 4.0 mm.

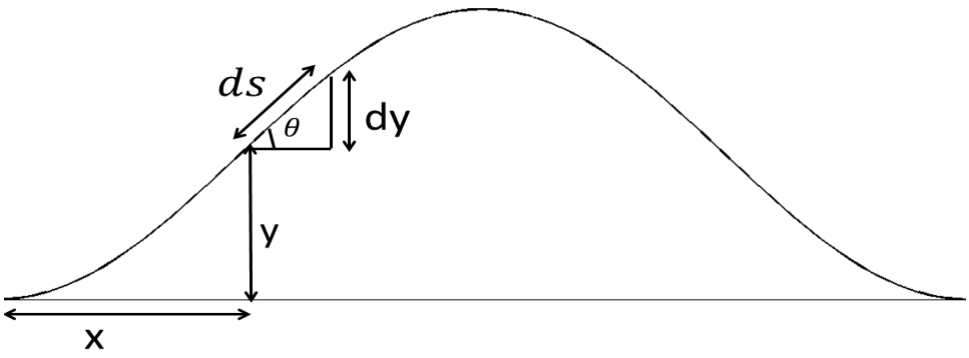

Figure 3.12: Sketch showing the center of mass of an undulation wave.

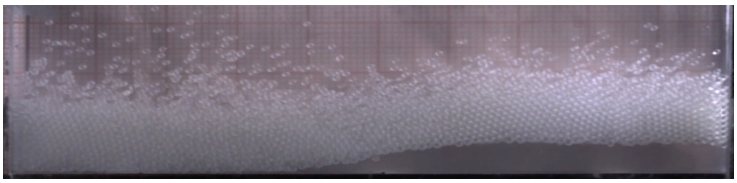

(a) n=1, $\Gamma = 9.3$

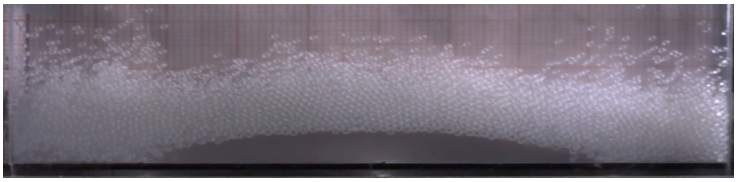

(b) n=2, $\Gamma = 10.43$

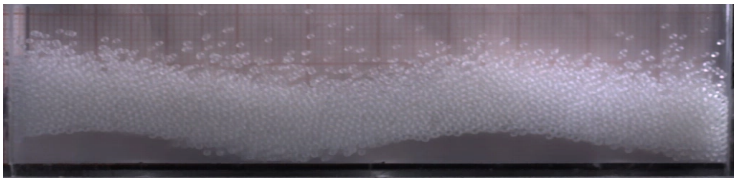

(c) n=3, $\Gamma = 12.24$

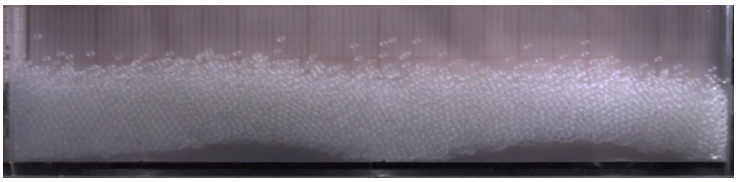

(d) n=4, $\Gamma = 13.86$

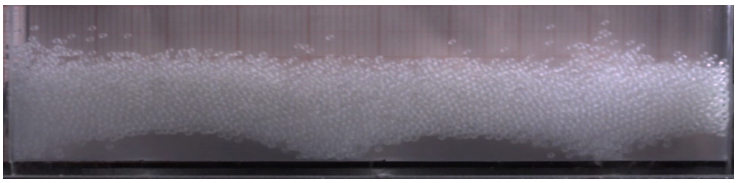

(e) n=5, $\Gamma = 14.88$

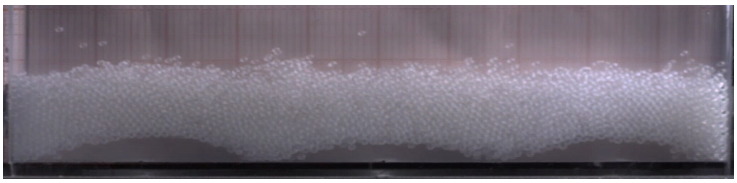

(f) n=6, $\Gamma = 16.3$

Figure 3.13: Six successive undulation modes for $F = 12$ layers of $d = 1.0\ mm$ glass balls at $A = 2.0\ mm$ with increasing frequency f =34, 36, 39, 41.5, 43, 45 Hz. The mode number n increases with the shaking acceleration.

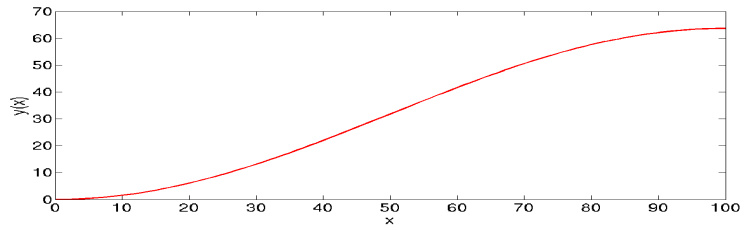

(a) n=1

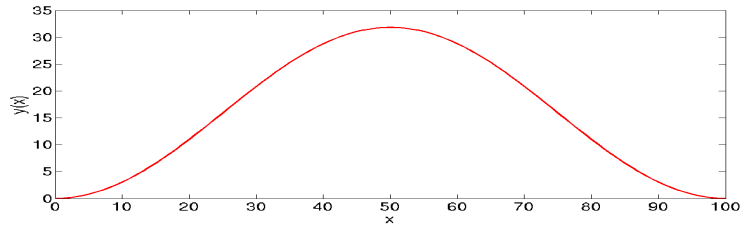

(b) n=2

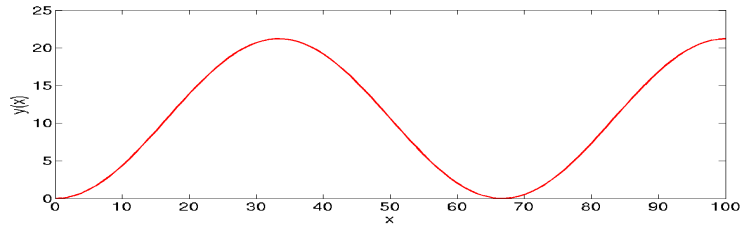

(c) n=3

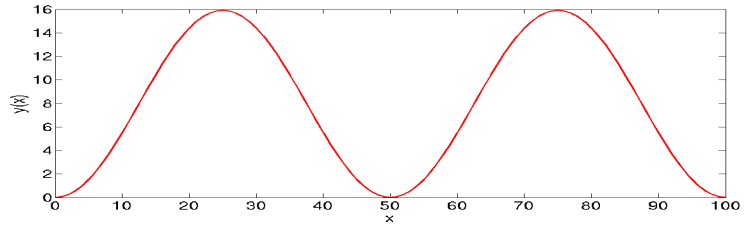

(d) n=4

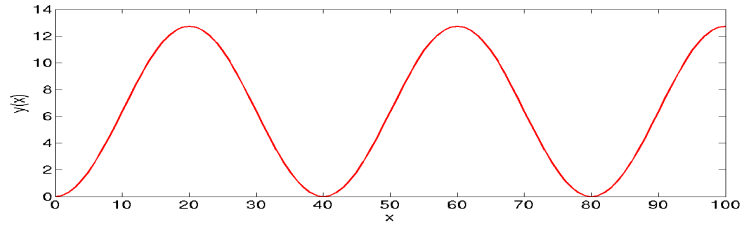

(e) n=5

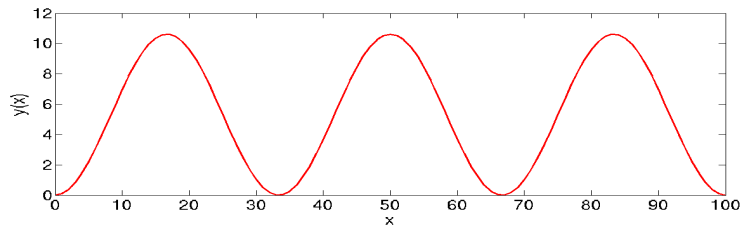

(f) n=6

Figure 3.14: Successive undulation profiles as generated by eqn. (3.5).

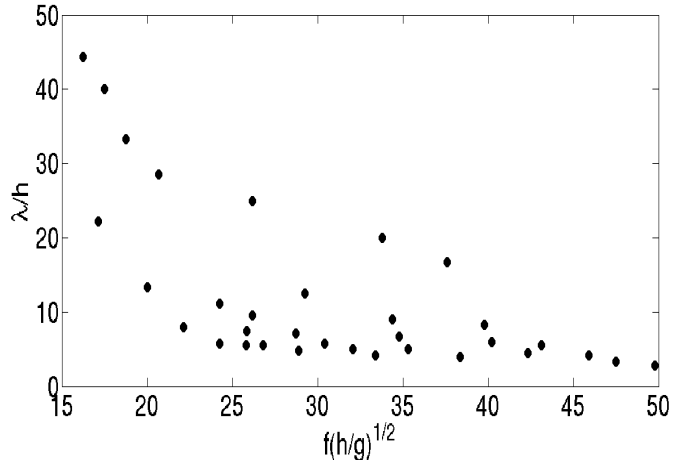

(a)

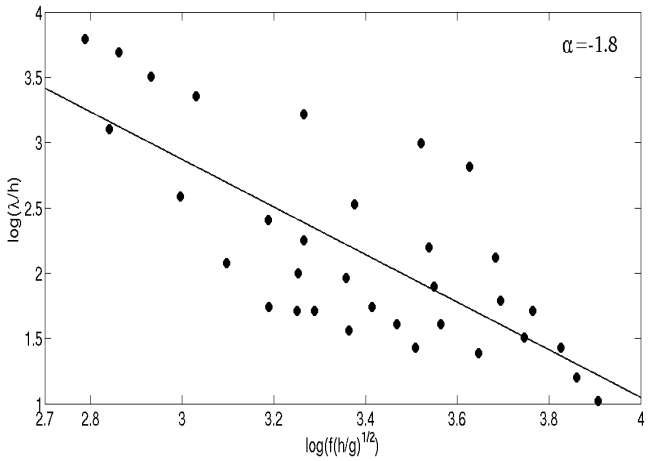

(b)

Figure 3.15: Dispersion relation for undulation waves.

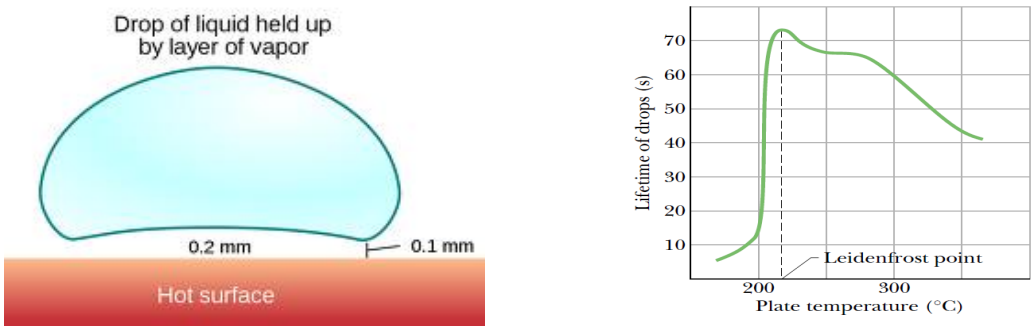

(a) (b)

Figure 3.16: (a) A sketch of the cross-section of a liquid drop hovering over its own vapor layer (taken from wikipedia), (b) The plot of survival time of a drop of distilled water versus different plate temperatures. The plot shows a peak at the Leidenfrost point of water (taken from [29]).

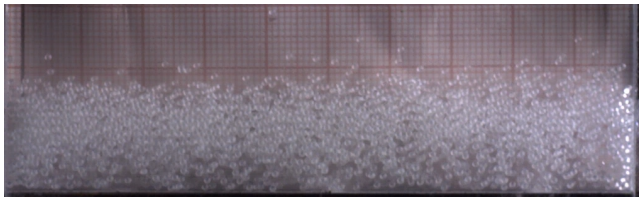

(a) t= 0T

(b) t= 0.5T

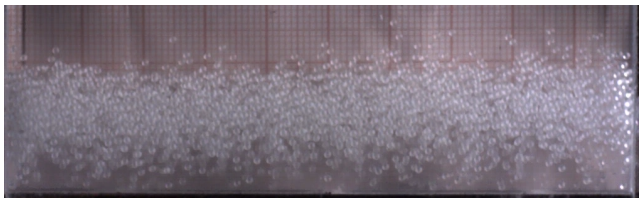

(c) t= 0.9T

Figure 3.17: Snapshots of the granular Leidenfrost state for $F = 6$ particle layers at $A = 4.0\ mm, f = 37$ Hz ($\Gamma = 22$ or $S = 88$). A dense cluster of particles is floating over a dilute layer of fast particles.

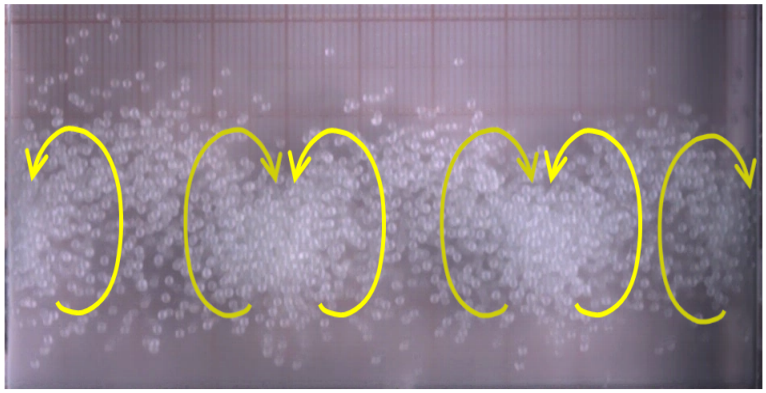

(a) t= 0T

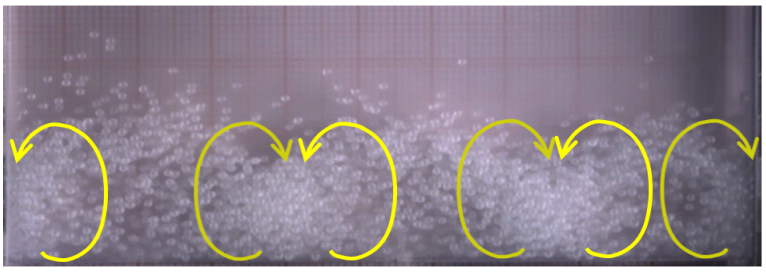

(b) t= 0.5T

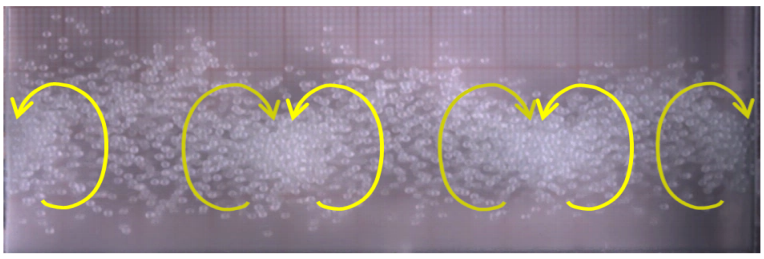

(c) t= T

Figure 3.18: Granular convection for $F = 6$ layers at $f = 57Hz$ and $A = 4.0\ mm$ (dimensionsless shaking acceleration $\Gamma = 52.3$), exhibiting six counter-rotating rolls.

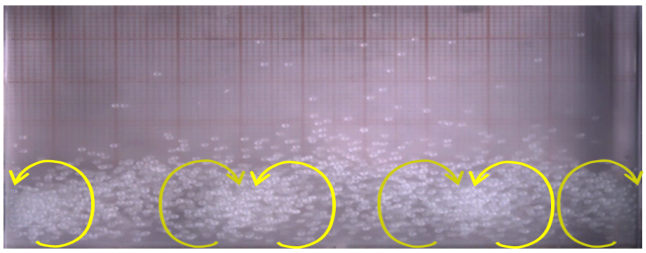

(a) $A = 3\ mm, f = 66$ Hz $(S = 157.76, \Gamma = 52.53)$

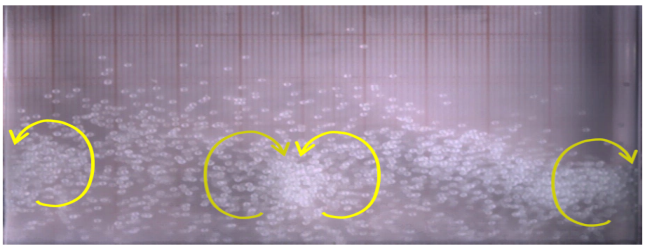

(b) $A = 4\ mm, f = 57$ Hz $(S = 209.2, \Gamma = 52.3)$

Figure 3.19: Convection pattern for $F = 5$ layers of $d = 1.0\ mm$ glass balls at two different shaking strengths, S. As S increases the convection rolls expand and hence container can accomodate less number of rolls.

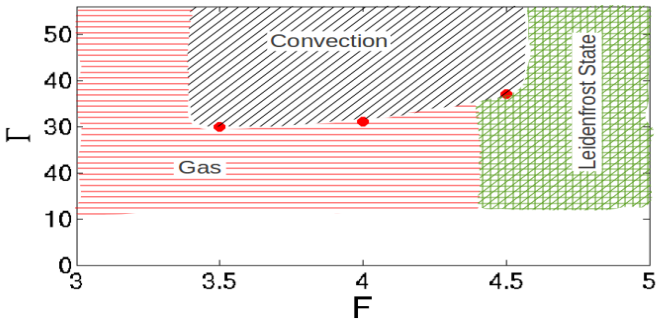

(a) $A = 2.0\ mm$

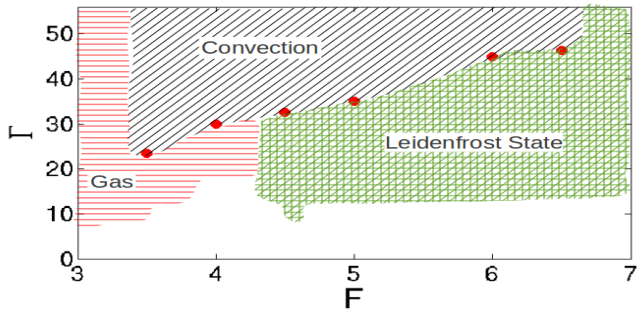

(b) $A = 3.0\ mm$

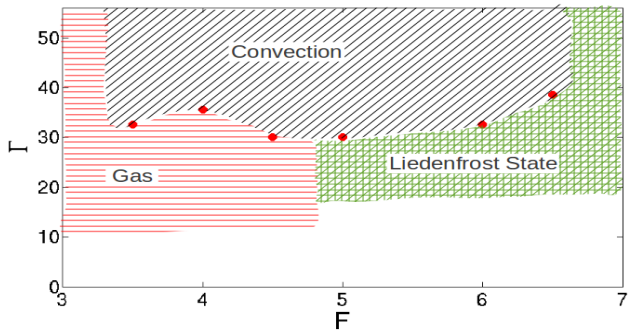

(c) $A = 4.0\ mm$

Figure 3.20: Transition to convection on $\Gamma - F$ plane: (a) transition from gaseous state ($3.5 \leq F \leq 4$) and from Leidenfrost state ($F = 4.5$) at shaking amplitude $A = 2.0\ mm$, (b) transition from gaseous state ($3.5 \leq F \leq 4$) and from Leidenfrost state ($4.5 \leq F \leq 6.5$) at shaking amplitude $A = 3.0\ mm$, (c) transition from gaseous state ($3.5 \leq F \leq 4.5$) and from Leidenfrost state ($5 \leq F \leq 6.5$) at shaking amplitude $A = 4.0\ mm$.

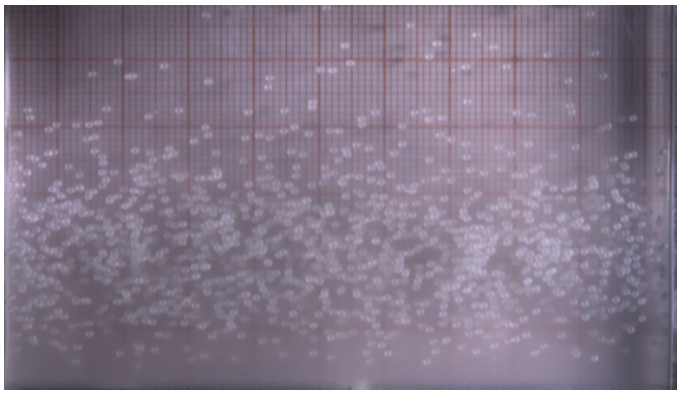

(a) t=0.0 T

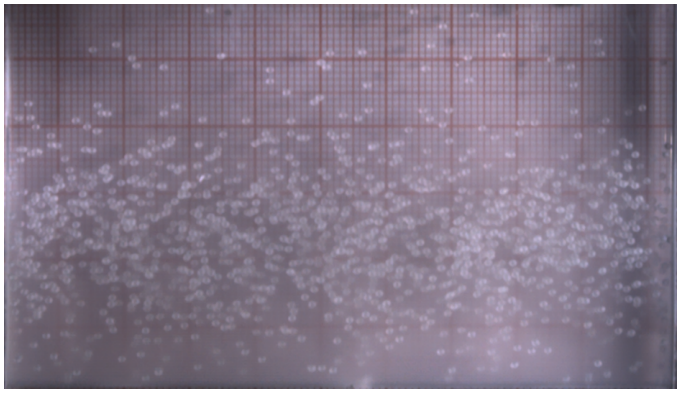

(b) t=0.3 T

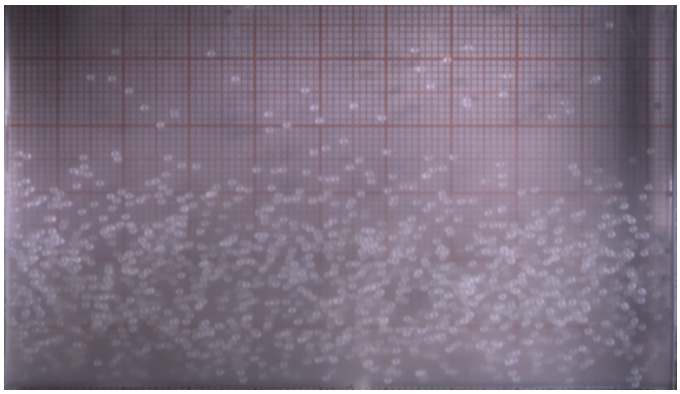

(c) t=0.8 T

Figure 3.21: Snapshots of Granular gas for $F = 3$ layers of $d = 1.0\ mm$ glass balls at shaking acceleration $\Gamma = 48.6$ ($A = 4.0\ mm, f = 55Hz$). This gaseous regime has been directly originated from bouncing bed.

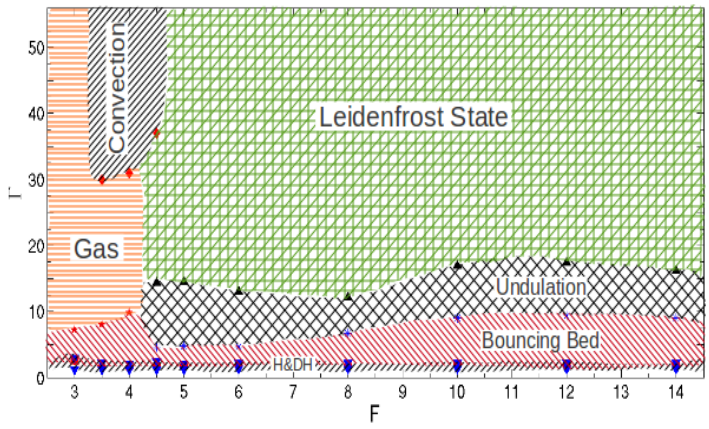

(a) $A = 2.0\ mm$

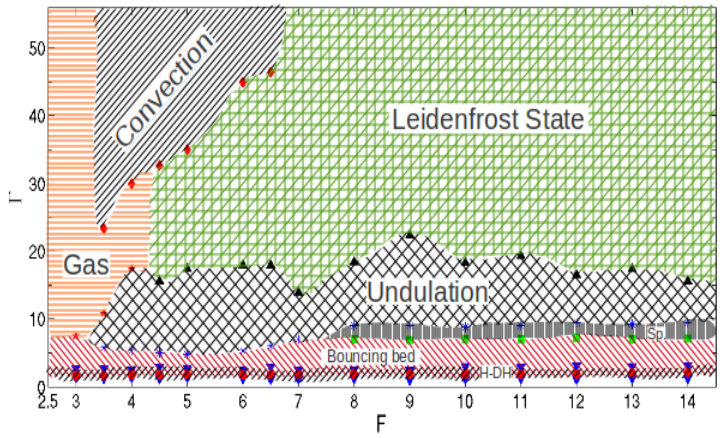

(b) $A = 3.0\ mm$

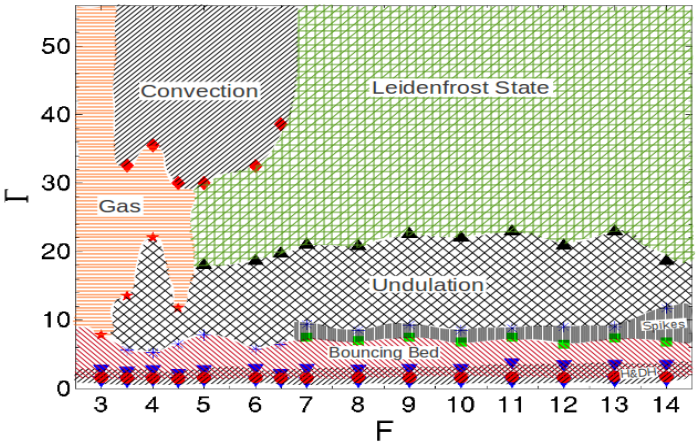

(c) $A = 4.0\ mm$

Figure 3.22: Phase diagram of vibrated bed at three constant shaking amplitude: (a)$A = 2.0\ mm$, (b)$A = 3.0\ mm$, and (c) $A = 4.0\ mm$.

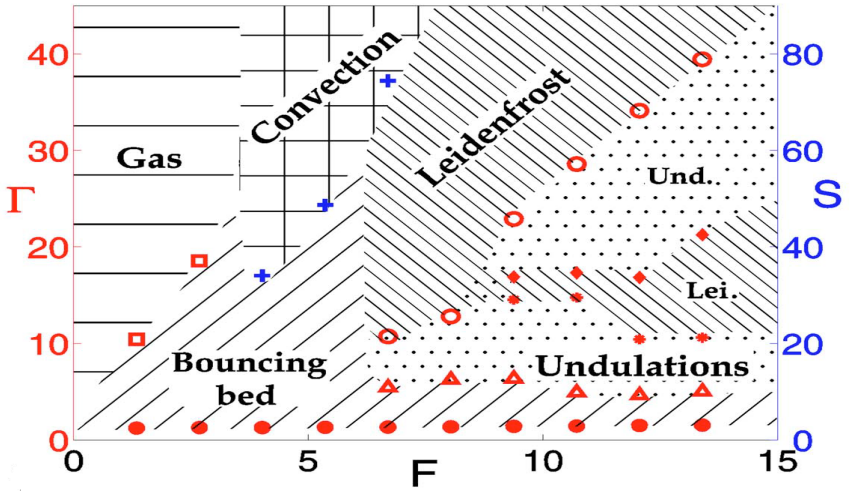

(a) $A = 2.0\ mm$

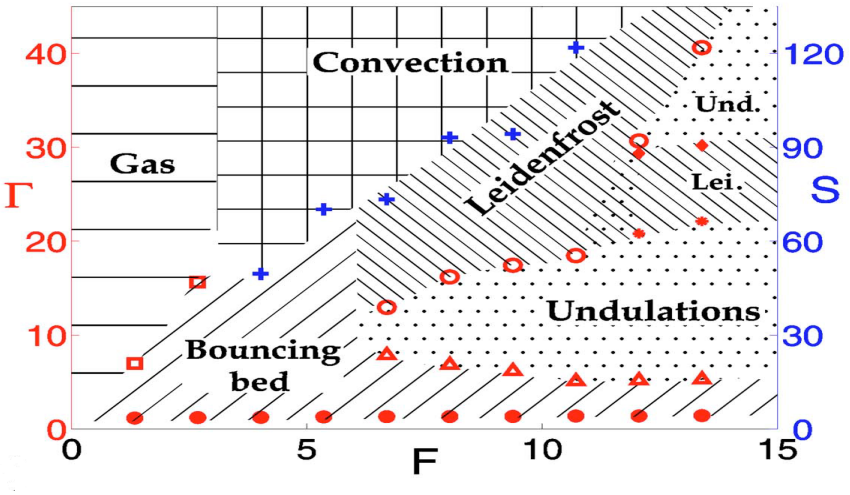

(b) $A = 3.0\ mm$

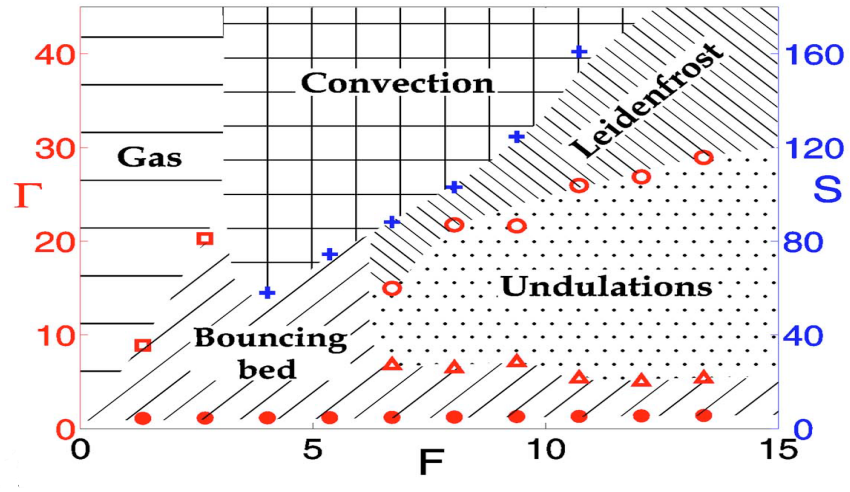

(c) $A = 4.0\ mm$

Figure 3.23: Phase diagram of Eshuis *et. al.* for vibrated bed at three constant shaking amplitude: (a)$A = 2.0\ mm$, (b)$A = 3.0\ mm$, and (c) $A = 4.0\ mm$ (taken from [7]).

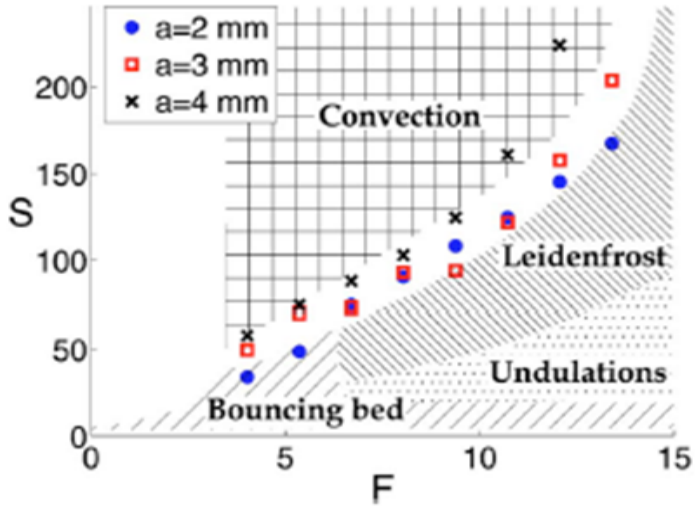

(a)

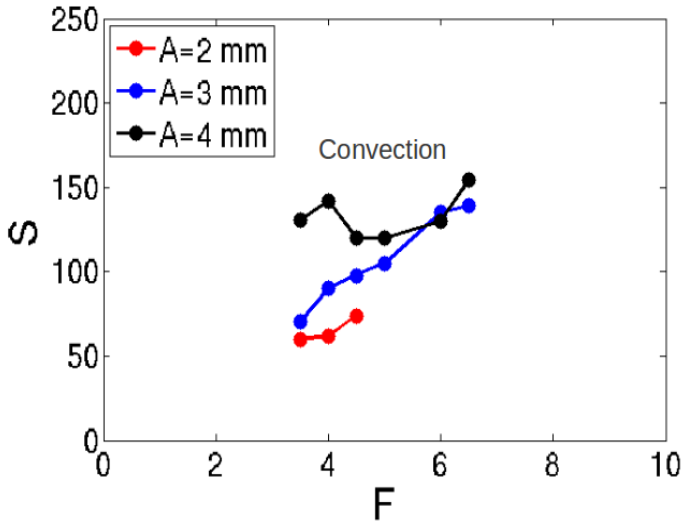

(b)

Figure 3.24: Transition towards granular convection for constant shaking amplitudes $A = 2.0\ mm,\ 3.0\ mm$ and $4.0\ mm$ on (S,F)-plane as obtained by (a) Eshuis *et. al.* (b) from our experiments.

CHAPTER 4

RESULTS FOR BINARY MIXTURE

In this chapter the experimental results of vertically vibrated binary granular mixture are discussed, with the culmination of all the results in phase diagrams. In section 4.2, the experiments on mixtures of steel and glass balls (both having diameters of $d = 1.0\ mm$) are discussed whereas in section 4.3 the experiments on mixtures of steel and delrin balls (both having diameters of $d = 1.0\ mm$) are discussed. The procedure of experiments is the same as in the case of monodisperse system (Chapter 3), where we gradually increased the shaking intensity at a constant shaking amplitude (A), except the difference that in the binary case we sweeped frequency (at constant A) both in upward and downward directions. The frequency sweep rate is also the same as in the monodisperse case (linear sweeping at 0.1 Hz/sec). We have considered equal layers of the two species (balls) constituting the binary mixture in both types of experiments, see Fig. 4.1. The total number of layers is given by

$$\begin{aligned} F &= F_s + F_d \\ F &= F_s + F_g. \end{aligned} \tag{4.1}$$

where F_s, F_g and F_d are the number of layers of steel, glass and delrin balls, respectively. Since the particles are of same size, this correspond to a 50:50 mixture of two species for both cases.

4.1 Results for Binary Mixture of Steel and Glass Balls

Experiments have been performed on steel and glass balls mixture at a constant shaking amplitude of $A = 3.0\ mm$ with frequency sweeping (linear sweep rate of 0.1 Hz/sec) in both upward and downward direction (see Fig. 4.1). While sweeping the frequency in downward direction, no *hysteresis* phenomenon has been observed.

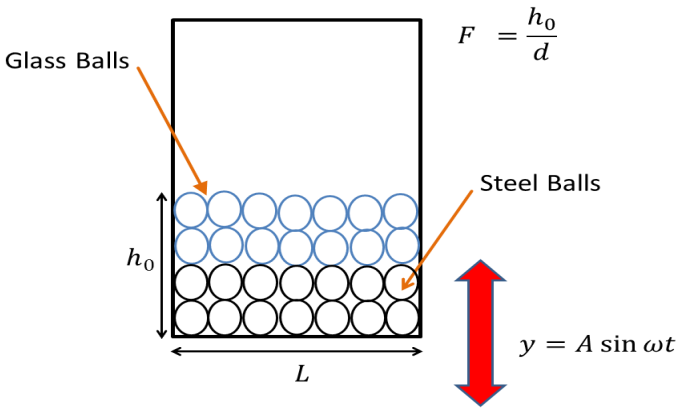

Figure 4.1: Sketch of vertically vibrated container holding bidisperse granular materials.

The density of steel balls is 7650 kg/m^3 and that of glass balls is 2500 kg/m^3. Therefore, the mass/density ratio of steel and glass balls is:

$$\frac{m_s}{m_g} = \frac{\rho_s}{\rho_g} = 3.06. \tag{4.2}$$

4.1.1 Bouncing bed

A series of snapshots for bouncing bed for a shaking amplitude of $A = 3.0$ mm with $F_s = 6$ and $F_g = 6$ particle layers are shown in Fig. 4.2. The explanation for the onset of bouncing bed is the same as in case of monodisperse system i.e. to detach the bed from the vibrating base, at some point of oscillation cycle the base should have downward acceleration greater than gravity plus the friction between the bed and the walls of the container. It is clear from the snapshots in Fig. 4.2 that the center of mass of steel balls is located at a larger height than that of glass beads. This is an exmaple of Brazil-nut segregation (BNS) [59], [60], [61].

The transition from solid to bouncing bed regime for a constant shaking amplitude is shown in Fig. 4.3 as a phase diagram in (Γ, F)-plane. It is seen that the onset value of Γ for transition to bouncing bed increases slowly with F in comparison to monodisperse case.

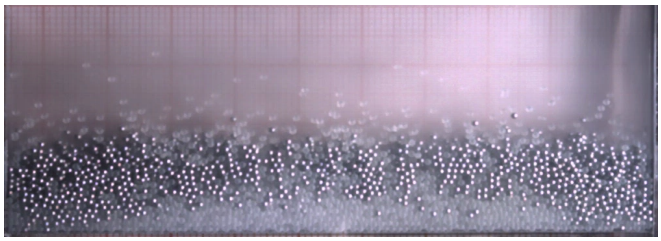

(a) t= 0T

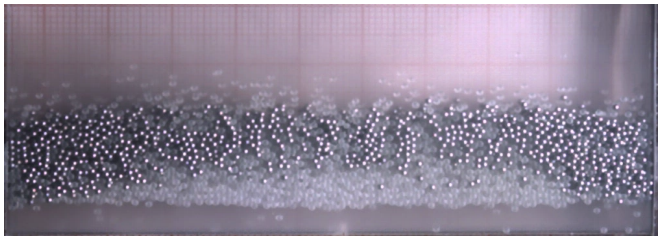

(b) t= 0.4T

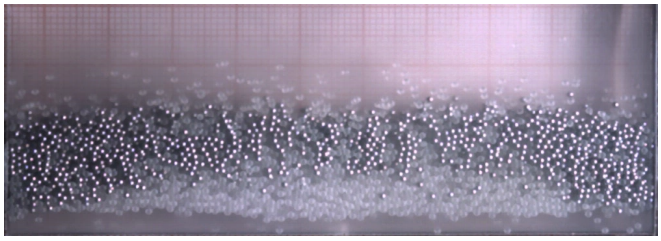

(c) t= 0.8T

Figure 4.2: Snapshots of bouncing bed at various time instants of oscillation cycle for $F_s = 6$, $F_g = 6$ layers of steel and glass balls of diameter $d = 1.0\ mm$ at $\Gamma = 3.48$ ($A = 3.0\ mm$, $f = 17\ Hz$). T=$1/f$ is the time period of shaking $y = A\sin(\omega t)$.

4.1.2 Undulation

The snapshots of undulation pattern exhibiting $n = 5$ mode are shown in Fig. 4.4. As evident from these snapshots, the undulation pattern takes one vibration cycle to exchange its maxima and minima positions and hence they are $f/2$ *waves*. It is interesting to note that both the steel and glass balls follow the same undulatory pattern and the center of mass of each species appears to be located at the same height. This implies that there is no segregation in this case and it is a well mixed undulation pattern.

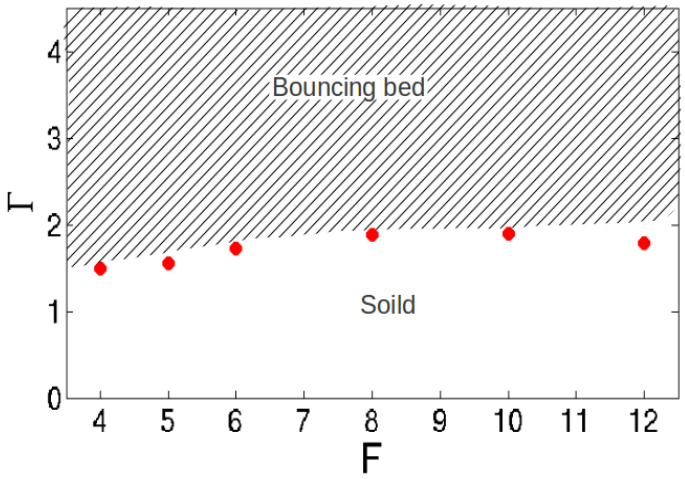

Figure 4.3: Transition to bouncing bed for 50:50 mixture of steel and glass balls of diameter 1.0 mm.

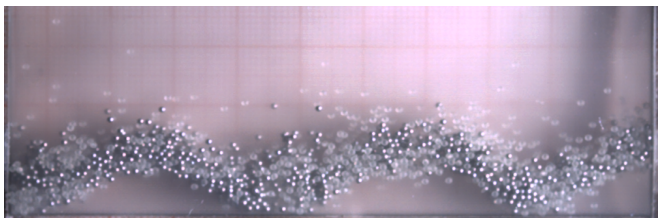

(a) t= 0T

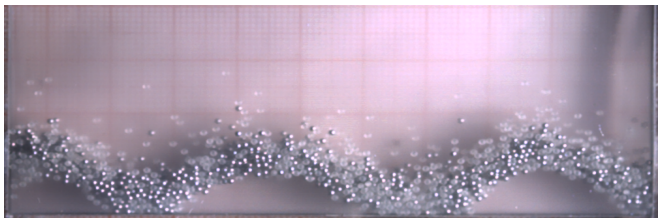

(b) t= T

Figure 4.4: Snapshot of one complete standing wave cycle ($n = 5$ mode) for $F_s = 2.5$, $F_g = 2.5$ layers of steel and glass balls of diameter $d = 1.0\ mm$ at $\Gamma = 8.16$ ($A = 3.0\ mm$, $f = 26\ Hz$).

4.1.3 Leidenfrost State

Fig. 4.5 shows two snapshots of Leidenfrost state for a 50:50 mixture of steel and glass balls at two locations during an oscillation cycle. It is clear from these

snapshots that there is horizontal segregation. Most of the steel balls have migrated to the right of the container. It appears that the center of mass for steel particles is located at a slightly greater height than that of glass balls; however this vertical segregation (Brazil-nut segregation, BNS) is very mild.

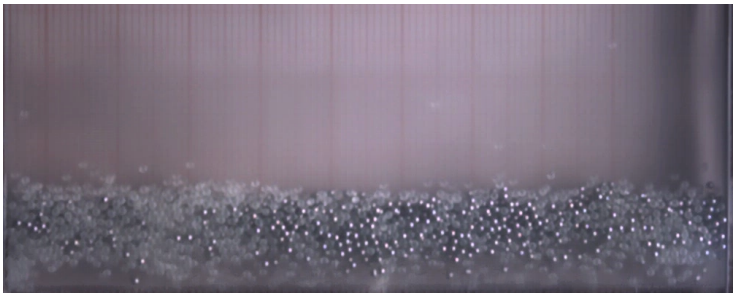

(a) $t = 0\mathrm{T}$

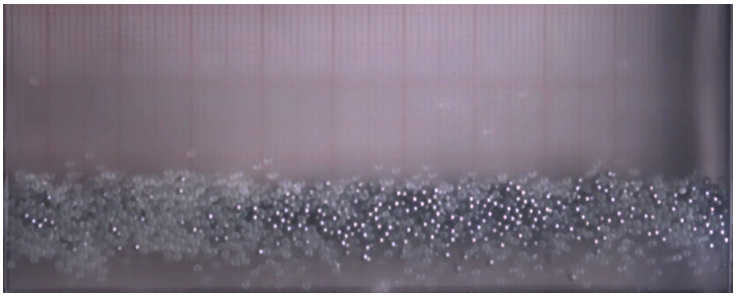

(b) $t = 0.9\mathrm{T}$

Figure 4.5: Snapshots of Leidenfrost state at two time instants of the oscillation cycle for $F_s = 3$, $F_g = 3$ layers of steel and glass balls of diameter $d = 1.0\ mm$ at $\Gamma = 51$ ($A = 3.0\ mm$, $f = 65\ Hz$).

4.1.4 Gaseous phase with partial Leidenfrost regime

Figure 4.6 shows two snapshots at $\Gamma = 51$ for $F = 5$ layers of particles. In this case we observe that the particles are showing a gaseous phase with a partial Leidenfrost state. Since the snapshots of Fig. 4.5 and 4.6 are reported at the same Γ-level ($\Gamma = 51$), it can be inferred that the gaseous phase has been trigerred due to the less number of particle layers ($F = 5$) in the latter case of Fig. 4.6. Note that the glass beads are horizontally segregated on the left of the container in Fig. 4.6 and are in a Leidenfrost state. On the other hand, the steel balls are segregated towards the right-wall of the container in Fig. 4.6 and are in a gaseous phase.

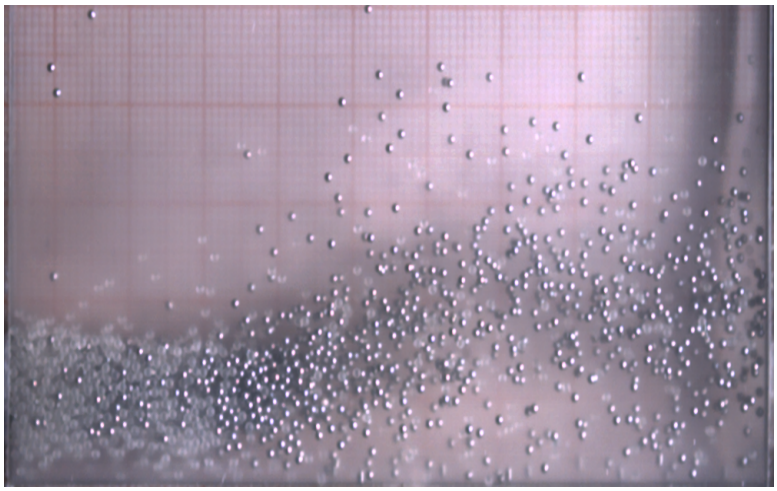

(a) $t = 0\mathrm{T}$

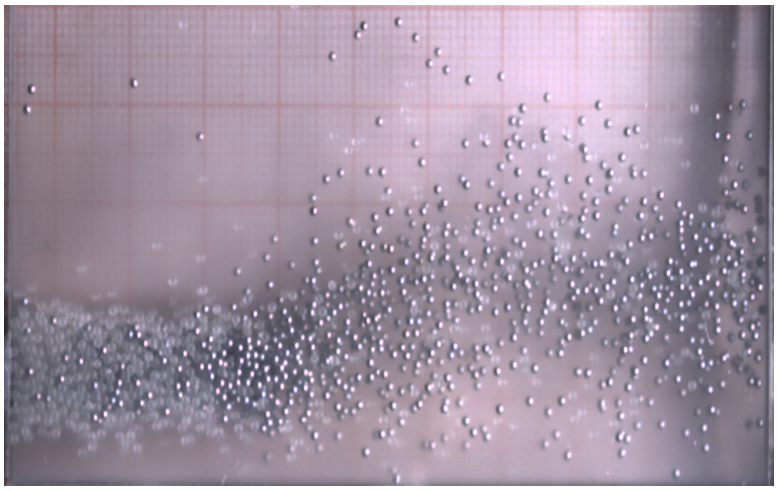

(b) $t = 0.9\mathrm{T}$

Figure 4.6: Snapshots of granular gas with partial Leidenfrost state and horizontal segregation at two time instants of oscillation cycle for $F_s = 2.5$, $F_g = 2.5$ layers of steel and glass balls of diameter $d = 1.0\ mm$ at $\Gamma = 51$ ($A = 3.0\ mm$, $f = 65\ Hz$).

4.1.5 Phase Diagram

The phase diagram for the 50:50 steel and glass balls mixtures has been obtained at a constant shaking amplitude of $A = 3.0\ mm$, via sweeping the frequency first in the upward direction upto maximum limit (defined by the shaker specified limit at $A = 3.0\ mm$) and then sweeping in the downward direction. Figure 4.7 shows the phase diagram while upsweeping the frequency at a constant shaking amplitude $A = 3.0\ mm$. While performing downsweeping experiments we observed no

hysteresis, therefore there is no difference between upsweeping and downsweeping phase diagrams. The undulation regime in Fig. 4.7 is relatively well mixed (i.e. no segregation). However, the other regimes in Fig. 4.7 are accompanied by vertical and horizontal segregation of steel and glass balls. These features are discussed below.

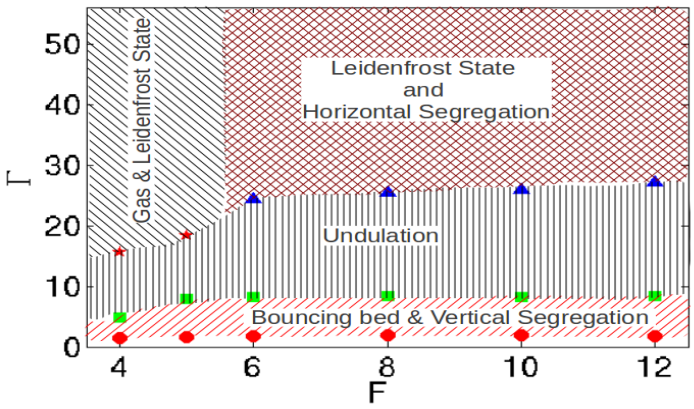

Figure 4.7: Phase diagram of equi-layer steel-glass balls binary mixture at constant shaking amplitude of $A = 3.0\ mm$.

For $F_g = 2$ and $F_s = 2$ ($F = 4$) layers of glass and steel balls in the phase diagram (see Fig. 4.7), if we increase the dimensionless shaking acceleration (Γ) at a constant shaking amplitude A by sweeping the frequency in the upward direction starting from a minimum ($5\ Hz$) we first observe a boucing bed, see Fig. 4.8 (for $\Gamma = 3.28$). Further increasing the Γ-level we observe the undulations, see Fig. 4.9 (for $\Gamma = 5.57$) and then next we reach the gaseous regime with a partial Leidenfrost state, see Fig. 4.10 (for $\Gamma = 24.4$). Similarly, if we fix the number of layers at $F_g = 4$ and $F_s = 4$ ($F = 8$) and increase the Γ-level at a constant shaking amplitude $A = 3.0\ mm$ we first observe bouncing bed, see Fig. 4.11 (for $\Gamma = 4.35$), next we observe undulations, see Fig. 4.12 (for $\Gamma = 9.5$) and finally a Leidenfrost state, see Fig. 4.13 (for $\Gamma = 52.5$). Similar to Fig. 4.5, the Leidenfrost state shows horizontal segregation of steel balls on both the corners of the container. The bouncing bed state in Fig. 4.11 clearly shows vertical segregation (BNS) and this is similar to Fig. 4.2. The undulatory wave states in Figs. 4.9 and 4.12 apear to be well mixed as confirmed previously in Fig. 4.4.

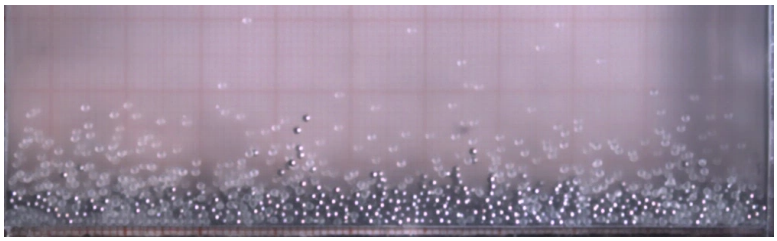

(a) $t = 0$ T

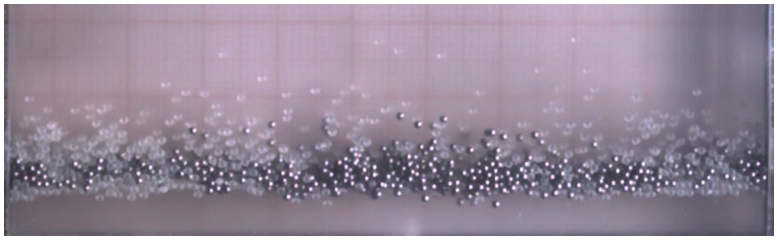

(b) $t = 0.9$ T

Figure 4.8: Snapshots of bouncing bed at two time instants of oscillation cycle for $F_s = 2$, $F_g = 2$ layers of steel and glass balls of diameter $d = 1.0\ mm$ at $\Gamma = 3.28$ ($A = 3.0\ mm$, $f = 16.5\ Hz$).

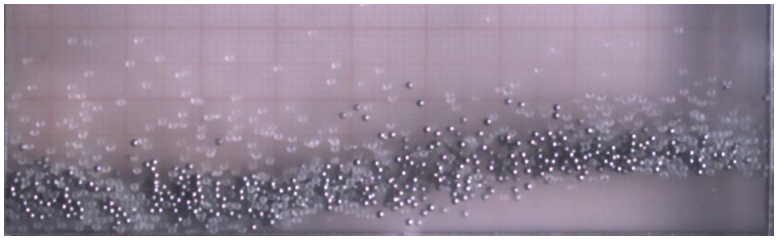

(a) $t = 0$ T

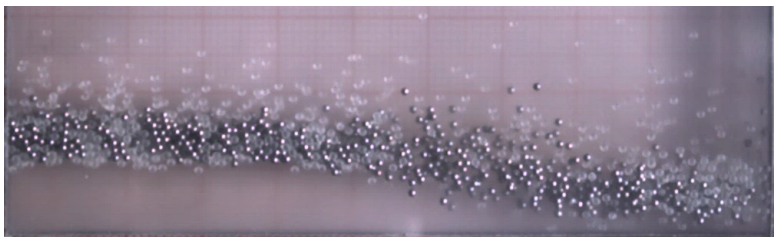

(b) $t =$ T

Figure 4.9: One complete standing wave cycle with $n = 1$ undulation mode for $F_s = 2$, $F_g = 2$ layers of steel and glass balls of diameter $d = 1.0\ mm$ at $\Gamma = 5.57$ ($A = 3.0\ mm$, $f = 21.5\ Hz$).

4.2 Results for Binary Mixture of Steel and Delrin Balls

Here we present results for binary mixtures of steel and delrin balls of both having diameters of 1.0 mm, see Fig. 4.14. The delrin balls are made of plastic, having a

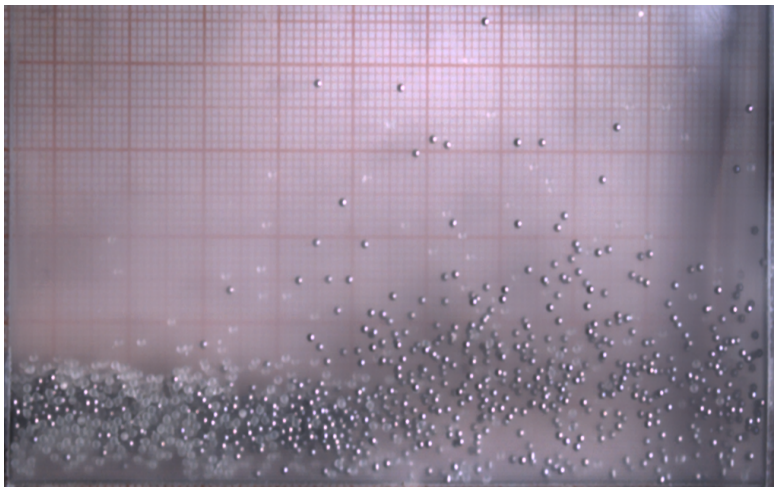

(a) $t = 0$ T

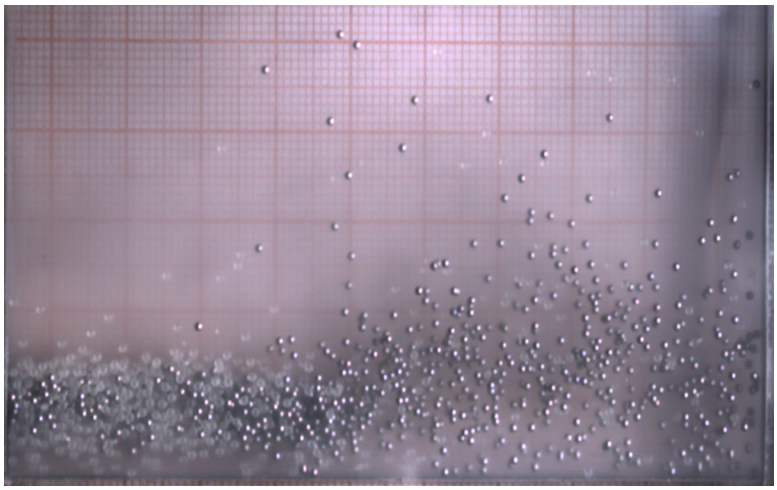

(b) $t = \mathrm{T}$

Figure 4.10: Snapshots of partial Leidenfrost effect with gaseous regime for $F_s = 2$, $F_g = 2$ layers of steel and glass balls of diameter $d = 1.0\ mm$ at $\Gamma = 24.4$ ($A = 3.0\ mm$, $f = 45\ Hz$).

density of $\rho_d = 1420 kg/m^3$. The mass and density ratio of steel and delrin balls is:

$$\frac{m_s}{m_d} = \frac{\rho_s}{\rho_d} = 5.38. \tag{4.3}$$

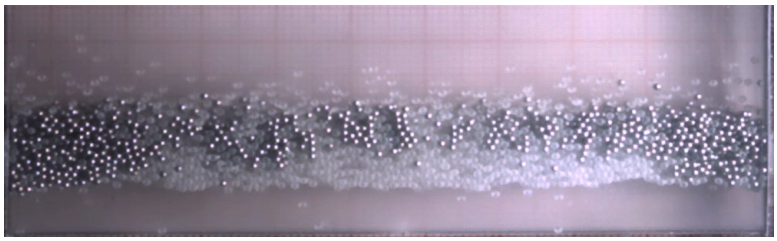

(a) $t = 0$ T

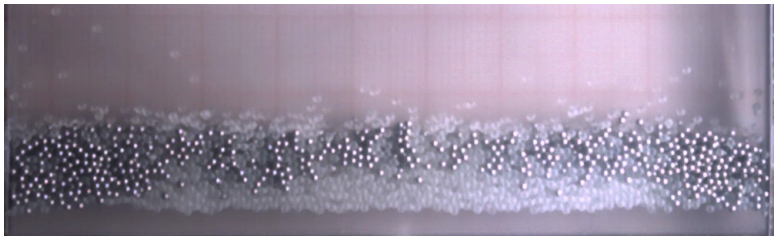

(b) $t = 0.85$ T

Figure 4.11: Snapshots of bouncing bed at various time instants of oscillation cycle with $F_s = 4$, $F_g = 4$ layers of steel and glass balls of diameter $d = 1.0\ mm$ at $\Gamma = 4.35$ ($A = 3.0\ mm$, $f = 19\ Hz$).

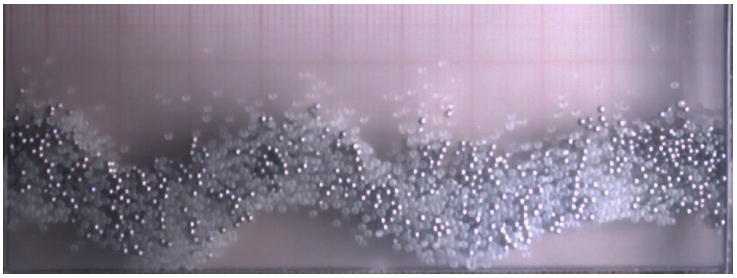

(a) $t = 0$ T

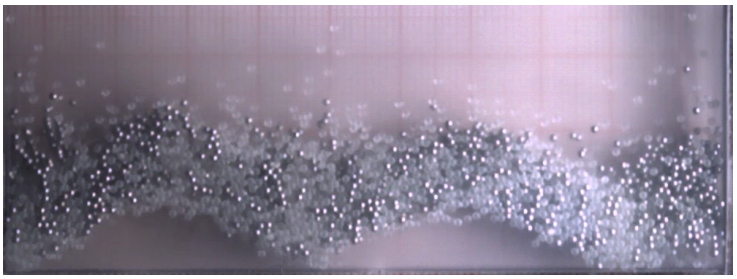

(b) $t = \mathrm{T}$

Figure 4.12: One complete standing wave cycle with $n = 4$ undulation mode for $F_s = 4$, $F_g = 4$ layers of steel and glass balls of diameter $d = 1.0\ mm$ at $\Gamma = 9.5$ ($A = 3.0\ mm$, $f = 28\ Hz$).

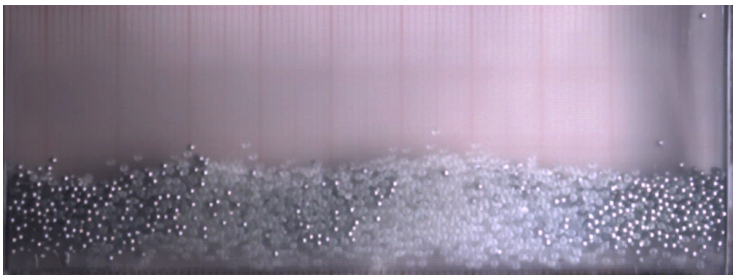

(a) $t = 0$ T

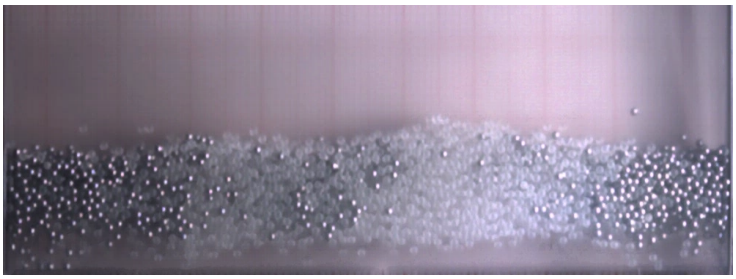

(b) $t = 0.9$ T

Figure 4.13: Snapshots of Leidenfrost state with horizontal segregation of steel balls at two time instants of oscillation cycle for $F_s = 4$, $F_g = 4$ layers of steel and glass balls of diameter $d = 1.0\ mm$ at $\Gamma = 52.5$ ($A = 3.0\ mm$, $f = 66\ Hz$).

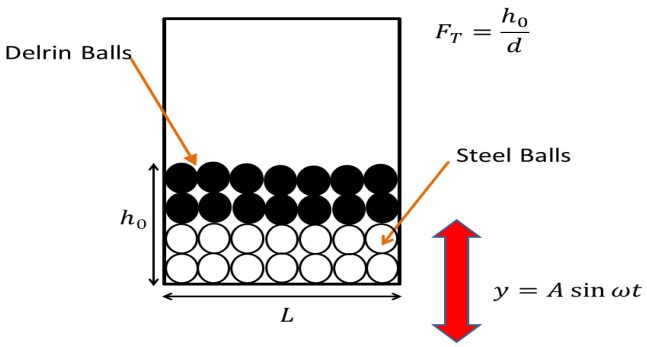

Figure 4.14: Sketch of vertically vibrated container holding bidisperse granular materials.

4.2.1 Bouncing bed and Undulation

A series of snapshots for the bouncing bed state is shown in Fig. 4.15. There seems to be both horizontal and vertical segregation of two species. On average, the delrin particles are at the top. This corresponds to reverse Brazil nut segregation (RBNS)

where lighter particles stay on top of heavier particles [59], [60].

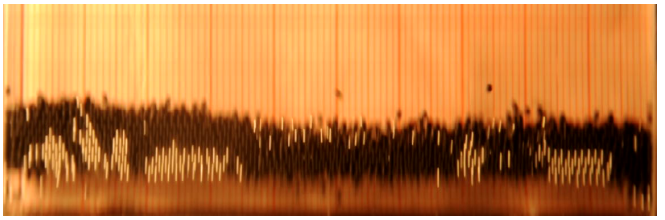

(a) $t = 0T$

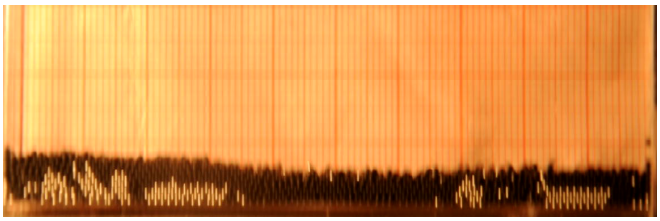

(b) $t = \frac{T}{2}$

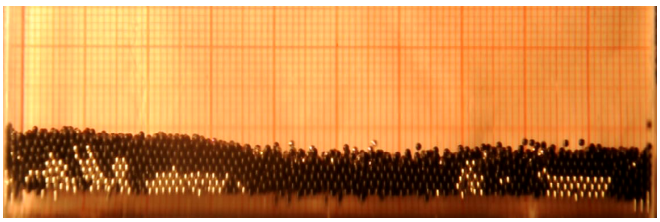

(c) $t = \frac{3T}{4}$

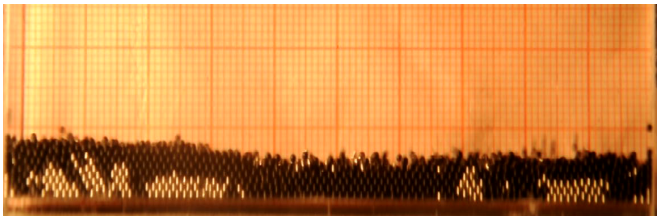

(d) $t = T$

Figure 4.15: Snapshots of bouncing bed at various time instants of oscillation cycle for $F_d = 3$ and $F_s = 3$ layers of delrin and steel balls at $\Gamma = 1.67$ ($A = 4.0\ mm$, $f = 10.2\ Hz$) while upsweeping. $T = 1/f$ is the time period of shaking.

The undulations or standing wave patterns have been observed with $n = 3$ and $n = 4$ mode as shown in the snapshots in Fig. 4.16 and Fig. 4.17, respectively. The particles in Fig. 4.17 appear to be well mixed and this corresponds to $\Gamma = 15$. The undulatory pattern in Fig. 4.16 corresponds to a relatively higher shaking intensity

at ($\Gamma = 17.5$). It is seen in Fig. 4.16 that some of the delrin (black) particles have been thrown out of the bed and they are floating at the top.

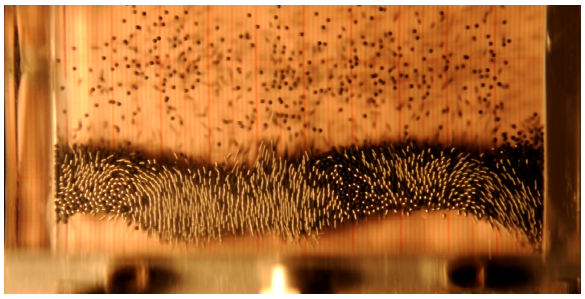

Figure 4.16: Snapshot of $n = 3$ undulation modes with $F_d = 7$ and $F_s = 7$ layers of delrin and steel balls at $\Gamma = 17.5$ ($A = 4.0\ mm, f = 33\ Hz$) while upsweeping.

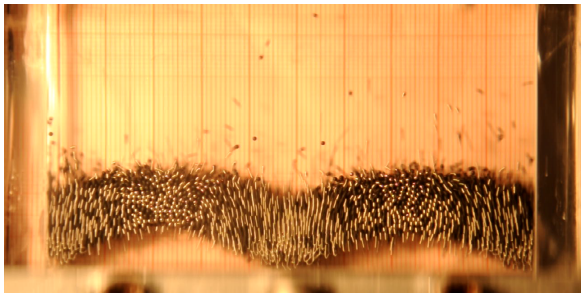

Figure 4.17: Snapshot of $n = 4$ undulation modes with $F_d = 6$ and $F_s = 6$ layers of delrin and steel balls at $\Gamma = 15$ ($A = 4.0\ mm, f = 30\ Hz$) while upsweeping.

4.2.2 Spikes (Ripples)

We observed spikes when the dimensionless shaking acceleration Γ is gradually increased into the bouncing bed regime as is clear in Fig. 4.18. It must be noted that the spikes show up only in the upsweeping experiment and absent in the downsweeping experiment.

4.2.3 Leidenfrost State and Segregation with Floating Cloud

A snapshot showing the Leidenfrost state during the upsweep experiment is shown in Fig. 4.19(a). Note that the delrin particles have segregated out in the vertical direction (see Fig. 4.13a). These segregated delrin particles have formed a cloud

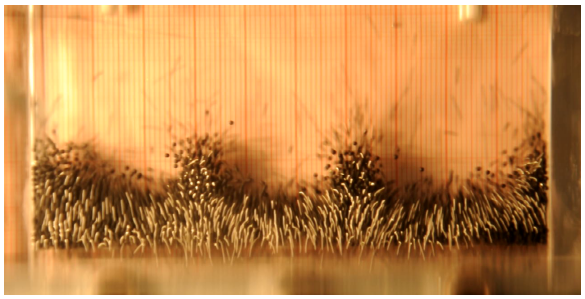

Figure 4.18: Snapshot of spikes (ripples) $F_d = 4$ and $F_s = 4$ layers of delrin and steel balls at $\Gamma = 8.25$ ($A = 4.0\ mm, f = 22.6\ Hz$) while upsweeping.

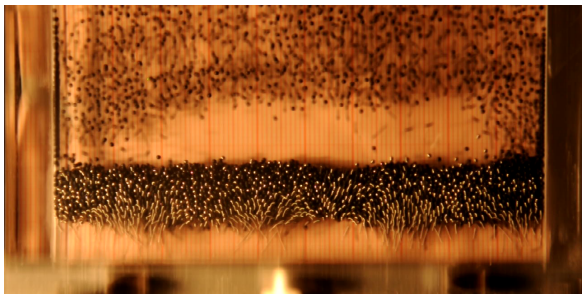

(a)

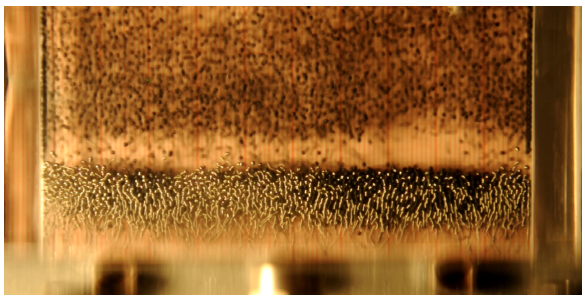

(b)

Figure 4.19: Snapshot of Leidenfrost State for $F_d = 7$ and $F_s = 7$ layers of delrin and steel balls at $\Gamma = 46.24$ ($A = 4.0\ mm, f = 53.6\ Hz$) while (a) sweeping frequency in upward direction (b)sweeping frequency in downward direction.

of floating particles and they survive during downsweeping, see Fig. 4.19(b). It has been verified that the floating particles stay close to front and back walls. The origin of this phenomena could possibly be due to electrostatic charging [62].

4.2.4 Convection and Segregation

Four counter-rotating convection rolls are seen in Fig. 4.20. It is observed that the convection rolls segregated out all the delrin particles from the mixture (see black particles at top in Fig. 4.20) and the convection is exhibited by the steel particles alone.

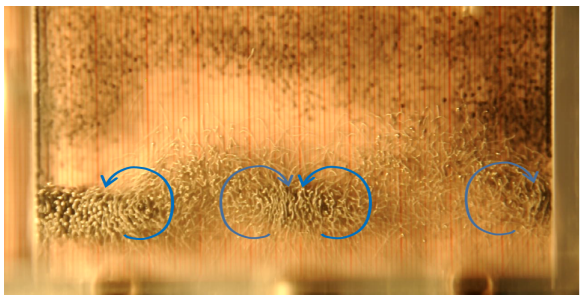

Figure 4.20: Snapshot of convection rolls with vertical segregation for $F_d = 5$ and $F_s = 5$ layers of delrin and steel balls at $\Gamma = 35.5$ ($A = 4.0\ mm, f = 47\ Hz$) while upsweeping.

4.2.5 Leidenfrost State with Bi-directional and Horizontal Segregation

Fig. 4.21(a) shows a snapshot of the Leidenfrost state exhibiting both vertical and horizontal segregation of delrin particles during upsweeping experiment. This state occurs at a relatively low shaking intensity of $\Gamma = 12$ in this figure.

The case of a partial Leidenfrost state coexisting with a granular gas and horizontal segregation of delrin particles is shown in Fig. 4.21(b). Note in Fig. 4.21(b) that the steel balls on the right of the container are in a gaseous state with hardly any delrin particles; most of the delrin particles have migrated to the left of the container and are in a Leidenfrost state. This coexistence of Leidenfrost and gaseous states occurs at a higher shaking intensity of $\Gamma = 55.65$ (Fig. 4.21).

4.2.6 Phase Diagrams

We have constructed phase diagrams for steel and delrin ball mixtures at a constant shaking amplitude of $A = 4.0\ mm$ by sweeping the frequency in the upward direc-

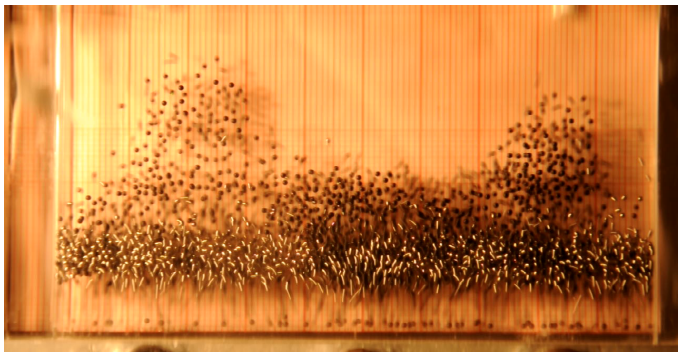

(a)

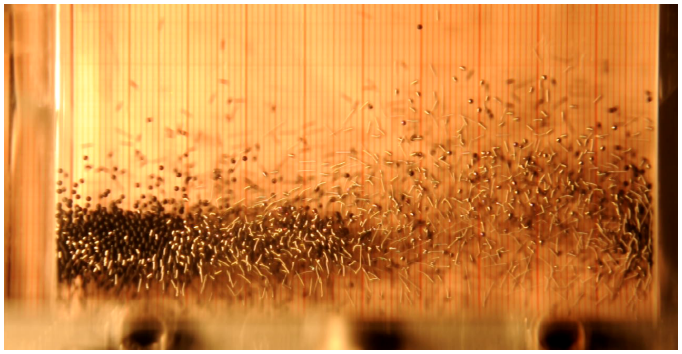

(b)

Figure 4.21: Snapshot of Leidenfrost State for $F_d = 3$ and $F_s = 3$ layers of delrin and steel balls with (a) Bi-directional segregation at $\Gamma = 12$ ($A = 4.0\ mm, f = 27.3\ Hz$) while upsweeping (b)Horizontal segregation and partial granular gas at $\Gamma = 55.65$ ($A = 4.0\ mm, f = 58.8\ Hz$) while downsweeping.

tion upto the maximum limit of $f = 59\ Hz$ (defined by the shaker specified limit at $A = 4.0\ mm$) and then sweeping in the downward direction. The phase diagrams, shown in Figs. 4.22(a) and 4.22(b), are much richer than those for monodisperse system as discussed in Chapter 3. There are also significant differences with the corresponding phase diagram in Fig. 4.7 for steel and glass ball mixtures.

It is clear from both phase diagrams in Fig. 4.22 that there is *hysteresis* i.e. there is a difference on the onset values of (Γ, F) for various patterns with increasing and decreasing Γ. We did not observe any spike structure while downsweeping, see the spike region in Fig. 4.22(a) around $\Gamma \sim 8$. The size of the Leidenfrost regime has increased while that of the undulation regime has decreased in comparison to the upsweeping case. One possible reason of this hysteresis phenomenon could be the floating particle cloud, where most of the delrin particles have vertically segregated

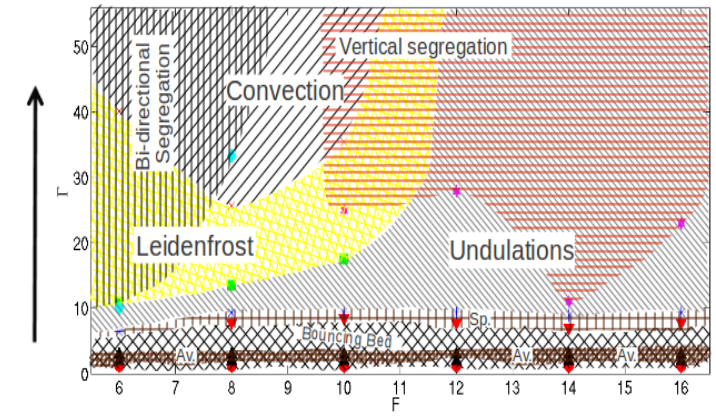

(a)

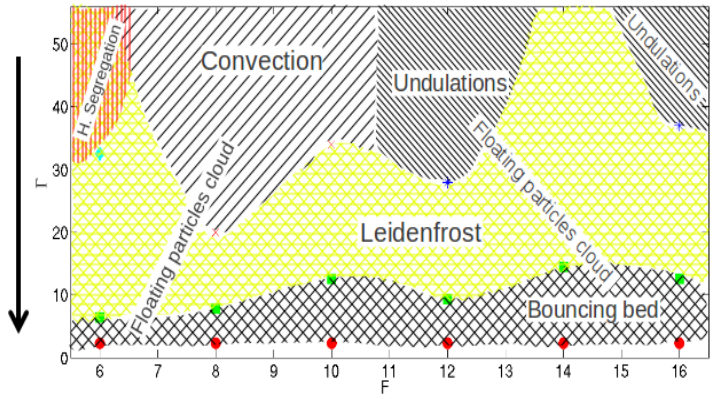

(b)

Figure 4.22: Phase diagram of equi-layer steel-delrin balls binary mixture, at constant shaking amplitude of $A = 4.0\ mm$ while: (a) upsweeping, (b) downsweeping.

out from the mixture and hence formed a cloud of delrin particles above. Hence, the regimes of different patterns shown in Fig. 4.22(b) during the downsweeping is less likely dominated by delrin particles because most of the delrin particles are floating up near the walls as shown in Fig. 4.19.

Figures 4.23(a) and 4.23(b) show undulation modes for $F_g = 8$ and $F_s = 8$ ($F = 16$) layers of steel and delrin balls for upsweeping and downsweeping, respectively, at a shaking intensity of $\Gamma = 49$. While the upsweeping case in Fig. 4.23(a) corresponds to a $n = 7$ mode undulatory wave, the downsweeping case in Fig.

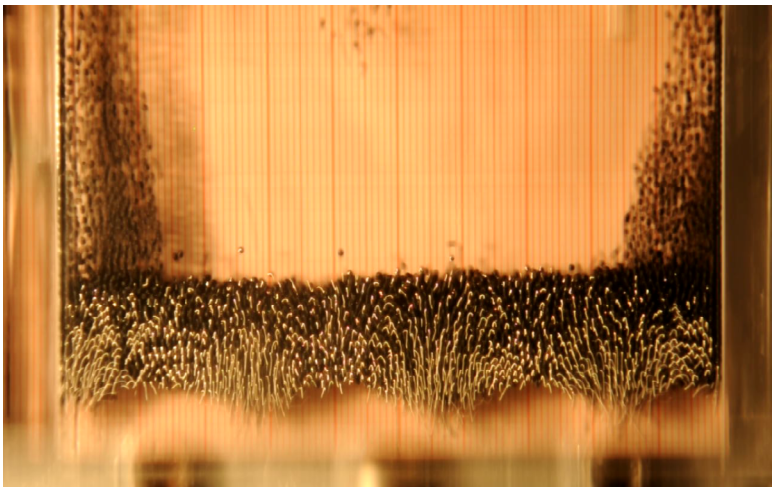

(a)

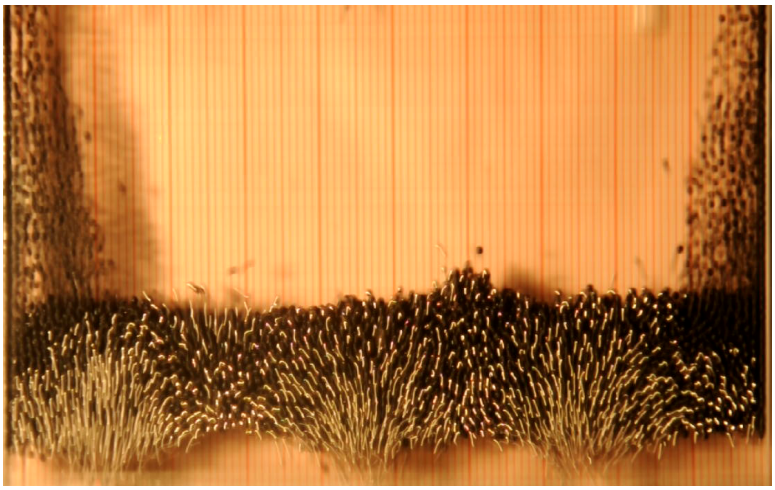

(b)

Figure 4.23: Snapshots of undulation pattern for $F_g = 8$ and $F_s = 8$ ($F = 16$) layers of steel and delrin balls for (a) upsweeping and (b) downsweeping for $\Gamma = 49$

2.3(b) corresponds to a $n = 6$ mode. This is another example of hysteresis. Such hysteresis phenomenon was absent for steel and glass ball mixtures as discussed in section 4.1. It is noteworthy in Figs. 4.23(a) and 4.23(b) that the floating clouds of delrin particles are confined to two sidewalls.

4.2.7 Possibility of electrostatic charging of Delrin particles.

Static electricty develops when two non-conducting materials rub against each other. Due to this rubbing one material gains electrons from the other and hence acquire negative and positive charges, thereby developing attraction [62]. We speculate that delrin balls and the perspex® container walls develops static charge due to which the delrin particles stick to walls. This is possibly the origin of floating cloud of delrin particles at sufficiently high shaking accelerations. This issue needs to be investigated in future.

CHAPTER 5

SUMMARY AND CONCLUSION

The present thesis dealt with an experimental study of vertically vibrated granular materials held in a quasi two-dimensional (2D) rectangular Perspex® container. Experiments are conducted on both monodisperse system (glass balls of diameter $d = 1.0\ mm$) and bidisperse mixtures. Two types of binary mixtures have been considered (1) the glass and steel balls both having diameters of $1.0\ mm$ and a density ratio of $\rho_s/\rho_g = 3.33$ and (2) the delrin and steel balls both having diameter $1.0\ mm$ and density ratio of $\rho_s/\rho_d = 5.56$). The dimensionless control parameters used to analyze the experiments are:

- The dimensionless shaking accelaration:

$$\Gamma = \frac{A\omega^2}{g}. \tag{5.1}$$

  where A is the shaking amplitude, $\omega = 2\pi f$ with f being the frequency and g is the acceleration due to gravity.

- **Number of ball layers at rest** F.

$$F = \frac{h_0}{d}, \tag{5.2}$$

  where h_0 is the bed height at rest. The number of layer in our experiments has been been varied from 3 to 16.

All the experiments were done by increasing the shaking intensity (measured in terms of dimensionless shaking acceleration Γ) while keeping the shaking amplitude A to be a constant. For a fixed number of particle layers, a gradual increase of the shaking intensity leads to transitions from one phenomenon to another at some critical value of Γ. All patterns have been presented as phase diagrams in the (Γ, F)-plane.

We have found various patterns in a shaken monodisperse system: bouncing bed, spiked structures (f/4 ripples), undulatory waves, granular Leidenfrost effect,

convection rolls and the granular gas. Most of our observed phenomena are found to be similar in characteristics to the observations made in the experimental study of Eshuis *et. al.* [7]. However, we found some differences with the work of Eshuis *et. al.* [7, 30, 58] as detailed below:

- For lesser mumber of particle layers F, we observed a transition to convection regime from the gaseous phase whereas Eshuis *et. al.* did not find such a transition.

- Eshuis *et. al.* observed a transition to convection from the bouncing bed regime which we did not find.

- We found spikes regime (f/4 ripples) for constant shaking amplitudes of $A = 3.0\ mm$ and $A = 4.0\ mm$. This spikes regime is sandwiched between the bouncing bed and the undulation regime. In contrast, the spikes regime is absent in phase diagrams of Eshuis *et. al.*

- We found the heaping and deheaping phenomena for low shaking intensities while going from the solid bed regime to the bouncing bed regime. This phenomenon was not observed by Eshuis *et. al.*

- Eshuis *et. al.* showed that the onset of convection for different shaking amplitudes collapse better in the (S, F)-plane. However, we did not find the above scaling.

The reasons for the differences between our study and that of Eshuis *et. al.*are not known at present, but this must be probed in a future work.

To our knowledge, the present thesis is the first comprehensive experimental study on pattern formation in shaken granular mixtures that covers a range of shaking intensities ($0 < \Gamma < 60$). We found many new patterns in two types of binary mixtures that we have studied: (a) the Leidenfrost state coexisting with a granular gas; (b) the Leidenfrost state showing horizontal segregation of two species; (c) the granular convection with a floating particle cloud; (d) vertical and horizontal segregations with other patterns. Examples of the first three phenomena are shown in Fig. 5.1(a), 5.1(b) and 5.1(c).

The phenomenon in Fig. 5.1(a) is an example of *phase separation* where only steel balls are in a gaseous phase on the right side of the container but the glass balls

are in a Leidenfrost state on the left. This is an unhitherto reported novel state of a shaken granular mixture at strong shakings. Although the vertical segregation of two species in a vertically shaken binary granular mixture is well-known in literature (Brazil-nut segregation or reverse Brazil-nut segregation), our finding of horizontal segregation within a Leidenfrost state in Fig. 5.1(b) is also new and novel. The phenomenon of "floating particle cloud" (see Fig. 5.1c) was found for the delrin and steel ball mixture for a wide range of parameters beyond the bouncing bed regime. We speculate that the possible origin of floating particle cloud could the generation of electrostatic charging of delrin balls– this issue needs a careful future study. Although we have found many new patterns, the underlying physics behind the formation of such novel patterns in binary granular mixtures remains to be explored in future.

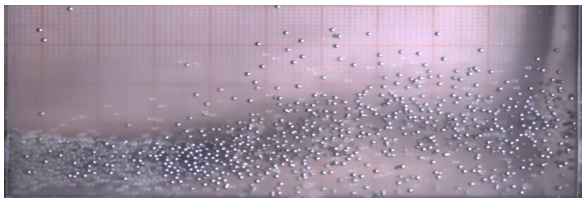

(a)

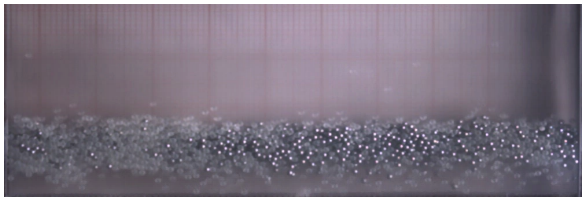

(b)

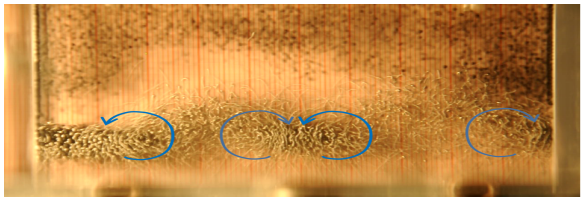

(c)

Figure 5.1: (a) Leidenfrost state with granular gas for $F_s = 2.5$ and $F_g = 2.5$ layers of steel and glass balls at $\Gamma = 51$. (b) Horizontal segregation with Leidenfrost state for $F_s = 3$ and $F_g = 3$ layers of steel and glass balls at $\Gamma = 51$. (c) Convection rolls with a floating cloud of particles for $F_d = 5$ and $F_s = 5$ layers of delrin and steel balls at $\Gamma = 35.5$.

References

[1] Ennis, B. J., Green, J., and Davies, R. Particle technology. The legacy of neglect in the U.S. Chem. Eng. Prog. 90, 32 (1994).

[2] Bates, L. The need for industrial education in bulk technology. Bulk Solids Handl. 26, 464 (2006).

[3] Jaeger, H. M., Nagel, S. R., and Behringer, R. P. Granular solids, liquids, and gases. Rev. Mod. Phys. 68, 1259 (1996).

[4] Rao, K.K. & Nott, P.R. An introduction to granular flow. Cambridge University Press (2008).

[5] Jackson, R. Some features of the flow of granular materials and aerated granular materials. J. Rheol. 30, 907 (1986).

[6] Jaeger, H. M. and Nagel, S. R. Physics of the granular state. Science 255, 1523 (1992).

[7] Eshuis, P.,van der Weele, K.,van der Meer, D., Bos, R. & Lohse, D. Phase diagram of vertically shaken granular matter. Physics of Fluids 19, 123301 (2007).

[8] Melo, F., Umbanhowar, P.B., & Swinney, H.L. Transition to parametric wave patterns in a vertically oscillated granular layer. Phys. Rev. Lett. 72, 172 (1994).

[9] Melo, F., Umbanhowar, P.B., & Swinney, H.L. Hexagons, Kinks, and Disorder in oscillated granular layers. Phys. Rev. Lett. 75, 3838 (1995).

[10] Clément, E., Vanel, L., Rajchenbach, J. & Duran, J. Pattern formation in a vibrated granular layer. Phys. Rev. E 53, 2972 (1996).

[11] Metcalf, T.H., Knight, J.B. & Jaeger H.M. Surface patterns in shallow beds of vibrated granular material. Physica A 236, 202 (1997).

[12] Douady, S., Fauve, S. & Laroche, C. Subharmonic instabilities and Defects in a Granular Layer under Vertical Vibrations. Europhys. Lett. 8, 621 (1989).

[13] Edwards, W.S. & Fauve, S. Patterns and quasi-patterns in the Faraday experiment. J. Fluid Mech. 278, 123 (1994).

[14] Umbanhowar, P.B. & Swinney, H.L. Wavelength scaling and square/stripe and grain mobility transitions in vertically oscillated granular layers. Physica A 288, 344 (2000).

[15] Sano, O.,Ugawa, A. & Suzuki, K. Pattern Formation on the Vertically Vibrated Granular Layer. Forma 14, 321 (1999).

[16] Bizon, C., Shattuk, M.D., Swift, J.B., Mc Cormick, W.D. & Swinney, H.L. Patterns in 3D Vertically Oscillated Granular Layers: Simulation and Experiment. Phys. Rev. Lett. 80, 57 (1998).

[17] Ugawa, A., & Sano, O. Dispersion relation of standing waves on a vertically oscillated thin granular layer. Journal of the Physical Society of Japan 71, 2815 (2002).

[18] Umbanhowar, P.B., Melo, F., & Swinney, H.L. Localised excitations in a vertically vibrated granular layer. Nature 382, 793-796 (1996).

[19] Carrillo, A.J., Pöschel, T., Salueña, C., Granular hydrodynamics and pattern formation in vertically oscillated granular disk layers. J. Fluid Mech. 597, 119 (2008).

[20] Pöschel, T., Schwager, T., & Salueña, C. Onset of fluidization in vertically shaken granular material. Phys. Rev. E 62, 1361 (2000).

[21] Renard, S., Schwager, T., Pöschel, T. & Salueña, C. Vertically shaken column of spheres. Onset of fluidization. Eur. Phys. J. E 4, 233 (2001).

[22] Luding, S., Clément, E., Rajchenbach, J. & Duran, J. Simulations of pattern formation in vibrated granular media. Europhys. Lett. 36, 247252 (1996).

[23] Luding, S. Surface waves and pattern formation in vibrated granular media. In Powders and Grains p.373. Balkema (1997 a).

[24] Aoki, K. M. & Akiyama, T. Spontaneous wave pattern formation in vibrated granular materials. Phys. Rev. Lett. 77, 4166 (1996).

[25] Bizon, C., Shattuk, M.D., Swift, J.B. Linear stability analysis of a vertically oscillated granular layer. Phys. Rev. E 60, 7210 (1999).

[26] Sano, O. Dilatancy, buckling, and undulations on a vertically vibrating granular layer. Phys. Rev. E 72, 051302 (2005).

[27] Sano, O. Solid-Fluid transition and the formation of ripples in vertically oscillated granular layers. AIP Conf. Proc. 1227, 100 (2010).

[28] Leidenfrost. G.J. On the fixation of water in diverse fire. Int. J. of Heat and Mass Transfer 9,1153 (1966).

[29] Walker. J. Boiling and the leidenfrost effect. leidenfrost essay.pdf.

[30] Eshuis, P., van der Weele, K., van der Meer, D., & Lohse, D. Granular Leidenfrost effect: Experiment and theory of floating particle clusters. Phys. Rev. Lett. 95, 258001 (2005).

[31] Chandrasekhar, S. Hydrodynamic and Hydromagnetic Stability Oxford University Press, Oxford, England. (1961).

[32] Bodenschatz, E., Pesch, W. & Ahlers, G. Recent developments in Rayleigh-Bènard convection. Annu. Rev. Fluid Mech. 32, 709 (2000).

[33] Ahlers, G., Grossman, S., & Lohse, D. Heat transfer and large scale dynamics in turbulent Rayleigh-Bènard convection. Review of Modern Physics, 81(2), 503 (2009).

[34] Clément, E. & Rajchenbach, J., Fluidization of a bidimensional powder, Europhys. Lett. 16, 133 (1991).

[35] Knight, J.B., Jaeger, H.M. & Nagel, S.R. Vibration-induced size separation in granular media: The convection connection. Phys. Rev. Lett. 70, 3728 (1993).

[36] Ehrichs,E. E., Jaeger, H. M., Karczmar, G. S., Knight,J. B., Kuperman, V. Y. & Nagel, S. R. Granular convection observed by magnetic reso- nance imaging. Science 267, 1632(1995).

[37] Aoki, K. M., Akiyama, T., Maki, Y. & Watanabe, T. Convective roll patterns in vertically vibrated beds of granules. Phys. Rev. E 54, 874 (1996).

[38] Knight, J. B., Ehrichs, E.E., Kuperman, V. Y., Flint, J. K., Jaeger, H. M. & Nagel, S. R. Experimental study of granular convection. Phys. Rev. E 54, 5726 (1996).

[39] Hsiau, S. S. & Chen, C. H. Granular convection cells in a vertical shaker. Powder Technol. 111, 210 (2000).

[40] Wildman, R. D., Huntley, J. M. & Parker, D. J. Convection in highly fluidized three-dimensional granular beds. Phys. Rev. Lett. 86 3304 (2001).

[41] Gallas,J. A. C., Herrmann,H. J. & Sokolowski,S. Convection cells in vibrating granular media.Phys. Rev. Lett. 69, 1371 (1992).

[42] Taguchi,Y.-h. New origin of a convective motion: Elastically induced convection in granular materials. Phys. Rev. Lett. 69, 1367 (1992).

[43] Luding,S., Clément,E., Blumen,A., Rajchenbach, J. & Duran,J. The onset of convection in molecular dynamics simulations of grains. Phys. Rev. E 50, R1762 (1994).

[44] Aoki, K. M. & Akiyama,T. Control parameter in granular convection. Phys. Rev. E 58 4629 (1998).

[45] Ramírez, R., Risso, D. & Cordero,P. Thermal convection in fluidized granular systems, Phys. Rev. Lett. 85, 1230 (200)

[46] Sunthar, P. & Kumaran,V. Characterization of the stationary states of a dilute vibrofluidized granular bed. Phys. Rev. E 64, 041303 (2001).

[47] Talbot, J. & Viot, P. Wall-enhanced convection in vibrofluidized granu- lar systems, Phys. Rev. Lett. 89, 064301 (2002).

[48] Cordero, P., Ramirez, R. & Risso, D. Buoyancy driven convection and hysteresis in granular gases: Numerical solution. Physica A 327, 82 (2003).

[49] Hayakawa, H., Yue, S. & Hong, D. C. Hydrodynamic description of granular convection. Phys. Rev. Lett. 75, 2328 (1995).

[50] He, X., Meerson, B. & Doolen,G. Hydrodynamics of thermal granular convection. Phys. Rev. E 65, 030301 (2002).

[51] Ohtsuki, T. & Ohsawa, T. Hydrodynamics for convection in vibrating beds of cohesionless granular materials. J. Phys. Soc. Jpn. 72, 1963 (2003).

[52] Khain, E. & Meerson, B. Onset of thermal convection in a horizontal layer of granular gas. Phys. Rev. E 67, 021306 (2003).

[53] Miao, G., Huang, K., Yun, Y. & Wei, R. Active thermal convection in vibrofluidized granular systems. Eur. Phys. J. B 40, 301 (2004).

[54] Aranson, I.S., Meerson, B., Sasorov, P.V., Vinokur, V.M. Phase separation and coarsening in electrostatically driven granular media. Phys. Rev. Lett. 88, 204301 (2002).

[55] Goldhirsch, I. Rapid granular flows. Annu. Rev. Fluid Mech. 35, 267 (2003).

[56] Eggers J. Sand as Maxwells demon. Phys. Rev. Lett. 83, 5322 (1999).

[57] Goldhirsch, I., Zanetti, G. Clustering in- stability in dissipative gases. Phys. Rev. Lett. 70, 1619 (1993).

[58] Eshuis, P., van der Meer, D., Alam, M., Jan van Gerner, H., van der Weele, K. & Lohse, D. Onset of convection in strongly shaken granular matter. Phys. Rev. Lett. 104, 038001 (2010).

[59] Alam, M., Trujillo, L., & Herrmann, H.J. Hydrodynamic theory for reverse Brazil nut segregation and the non-monotonic ascension dynamics. Journal of Statistical Physics 124, 587 (2006).

[60] Trujillo, L., Alam, M., & Herrmann, H.J. Segregation in a fluidized binary granular mixture: Competition between buoyancy and geometric forces. Europhysics Letters 64, 190 (2003).

[61] Hong, D.C., Quinn, P.V. & Luding, S. Reverse Brazil nut problem: Competition between percolation and condensation. Phys. Rev. Lett. 86, 3423 (2001).

[62] Pähtz, T., Herrmann, H.J. & Shinbrot, T. Why do particle clouds generate electric charges? Nature Physics 6, 364 (2010).